The 4th School on High Energy Physics

26 April — 5 May, 2014

Ain Shams University (ASU) & The British University in Egypt (BUE)

Organized by

Egyptian Network of High Energy Physics (ENHEP)

Europe Egypt Network for Particle Physics (EENP2)

Gaseous detectors and applications II

P. Fonte

LIP-Coimbra

Outlook

Muon tomography

- Transmission muon tomography
- Scatter muon tomography
- Influence of design parameters in scatter muon tomography

RPC-PET

- Basic features of PET and RPC-PET
- Small animal RPC-PET
- Human whole-body RPC TOF-PET
- Image reconstruction

Transmission muon tomography

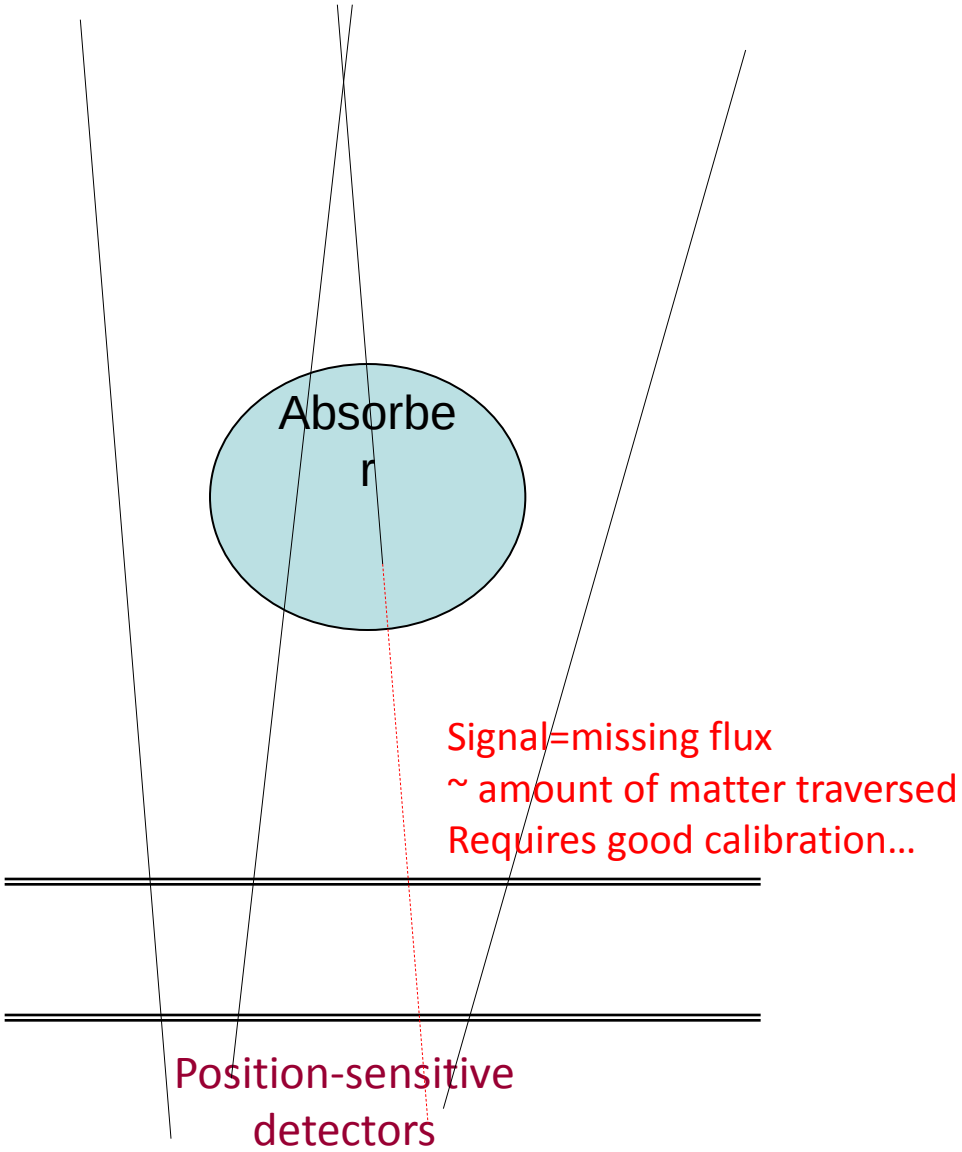

Most famous: L.Alvarez et al. @ Khafre's piramid

Transmission muon tomography - geotomography

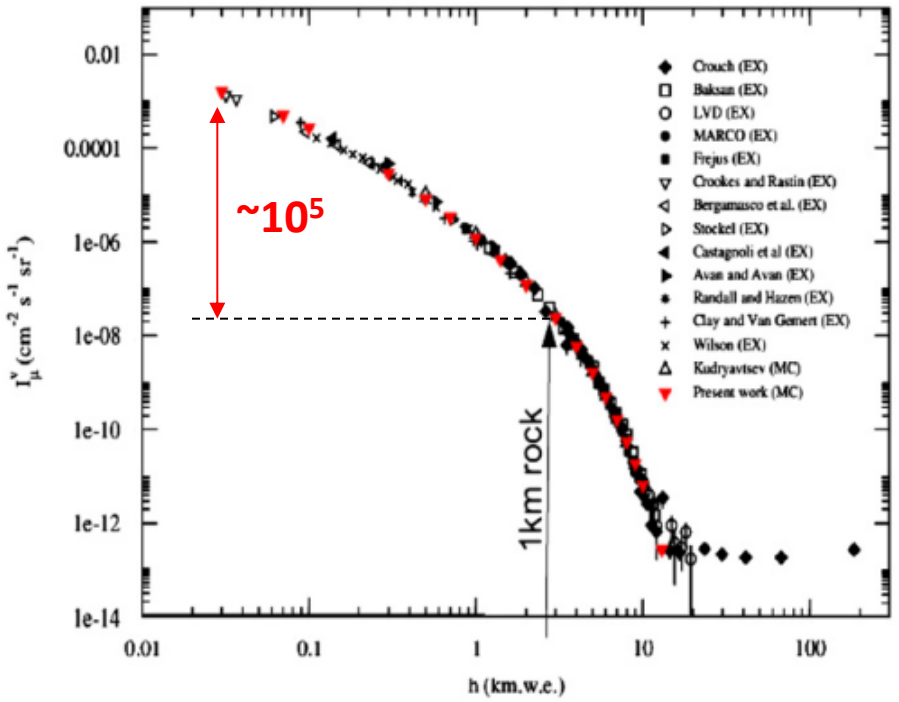

Fig. 2. Integrated flux computed as a function of the standard rock thickness L in metres-water-equivalent (m.w.e.) compared to experimental points.

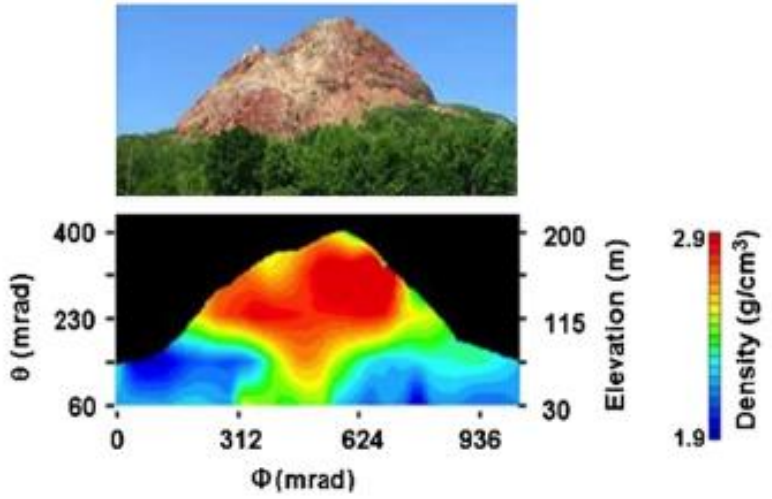

Fig. 7. Top: view of the Showa-Shinzan lava dome. Bottom: average density distribution projected onto the detector's plane.

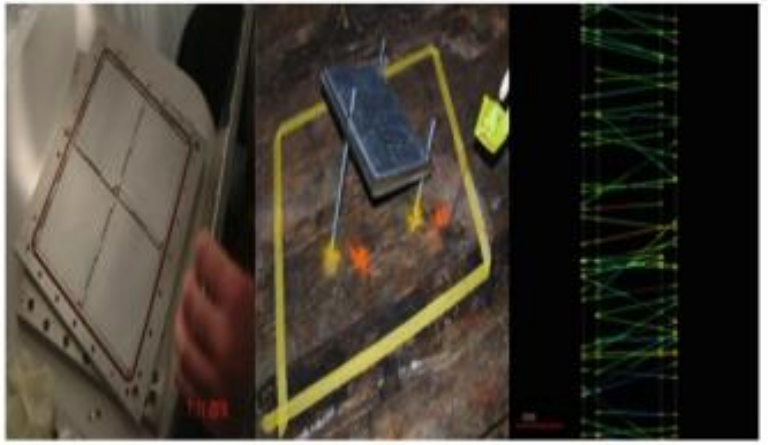

Fig. 8. Left: emulsion module hosting 16 emulsions. Middle: module station during data taking. Right: reconstructed passing-through tracks.

Detector=emulsion

Volcano tomography

[J. Marteau e tal. NIM A 2011]

Transmission muon tomography - geotomography

65.8 days of data taking, 0.16 m^2 x 0.5 m

Transmission coefficient

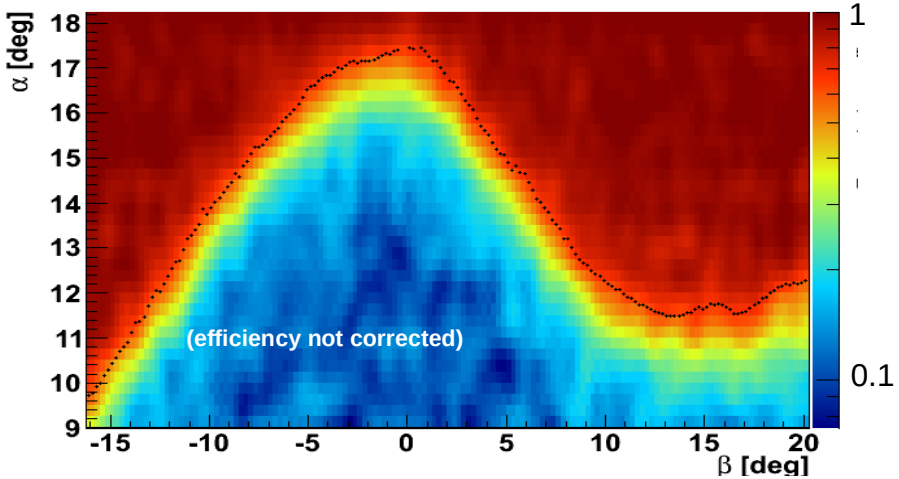

Opacity coefficient : "Density-like"

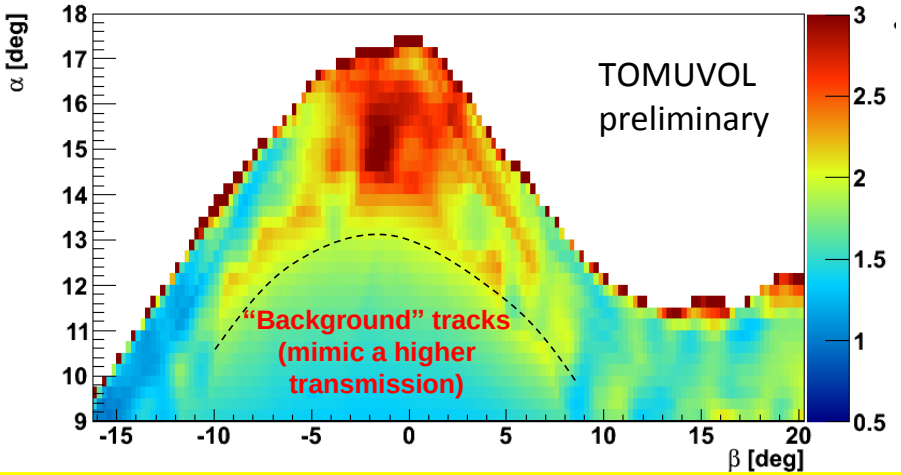

TOMUVOL project
Detector=RPC
@ Puy de Dome, France

Volcanoes Tomography With Atmospheric Muons
I. Laktineh et al. RPC2014

Hints of a structural contrast in the summit area. At the base, background mimics a higher transmission.

15

Absorption muon tomography - geotomography

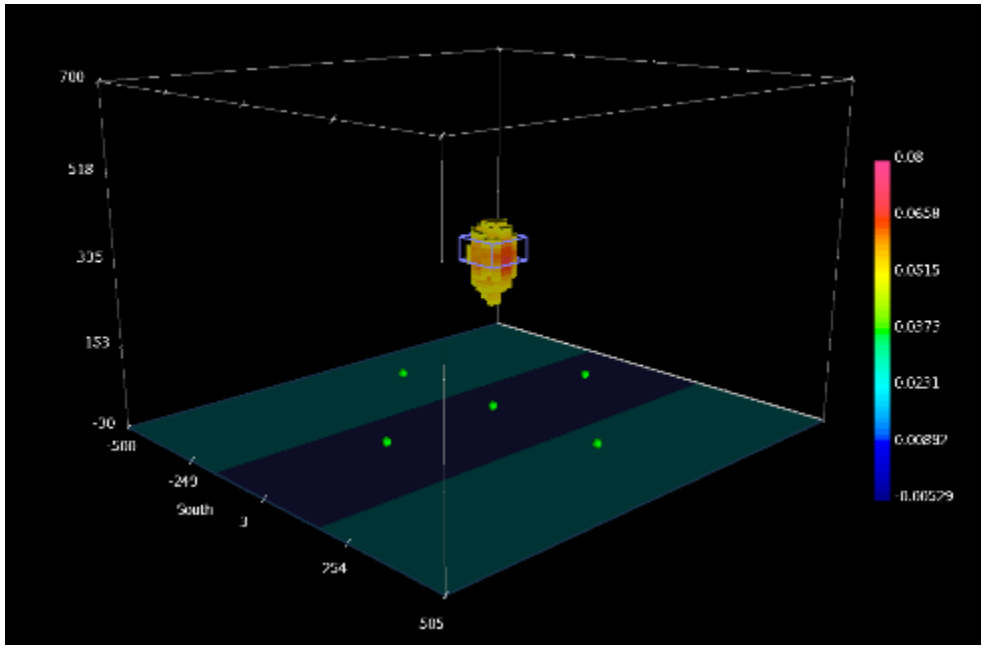

Detector=scintillator bars
Detection of dense ore deposits

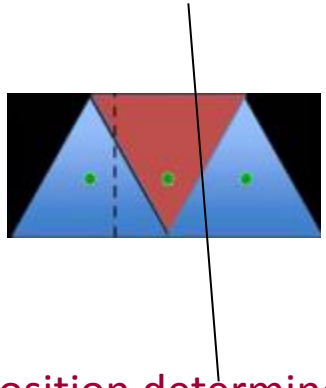

Position determined by the light-sharing

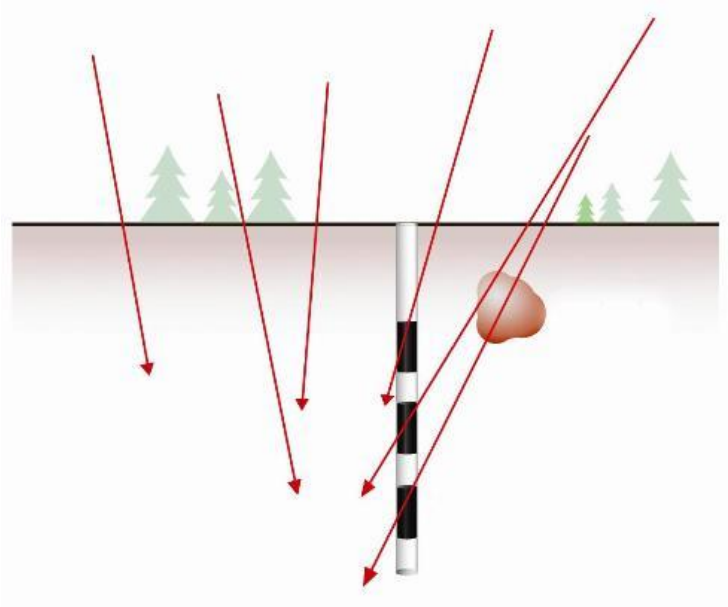

AAPS Advanced Applied Physics Solutions

ETPP Exploitation des Techniques de Pointe en Physique

http://www.aapsinc.com, Canada

Scatter muon tomography

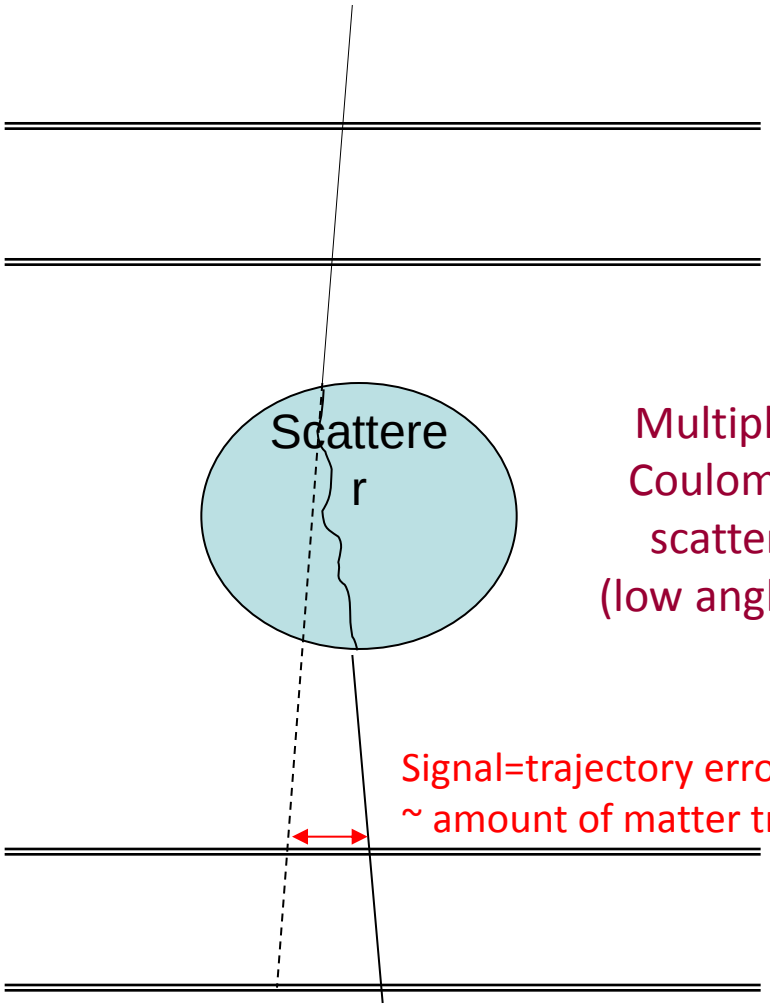

Multiple Coulomb scatter (low angles)

Signal=trajectory error
~ amount of matter traversed

Position-sensitive detectors

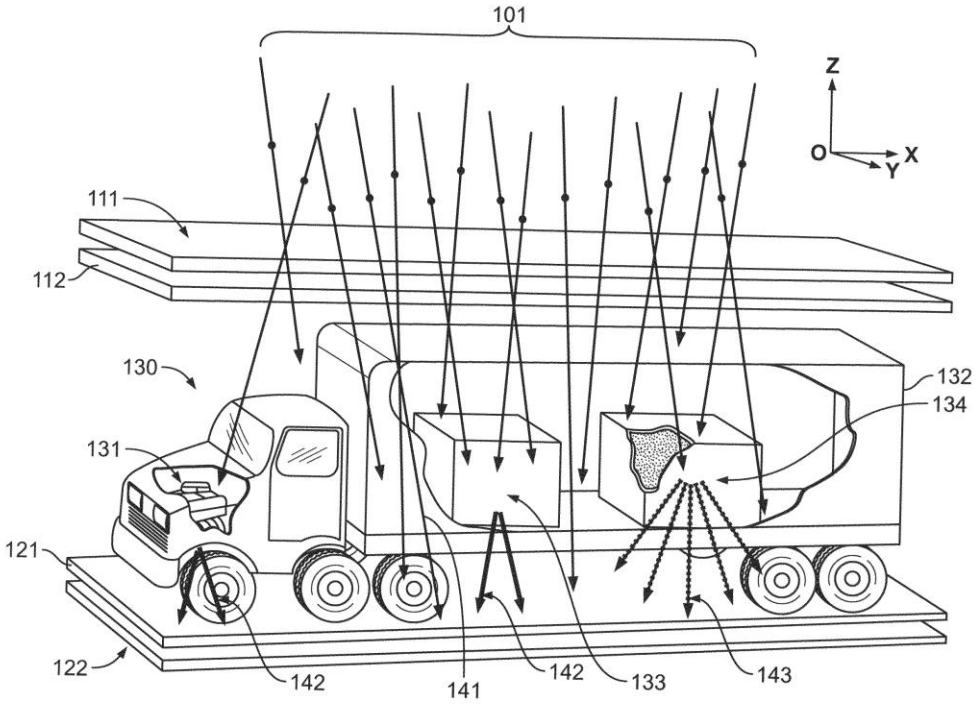

$$\theta_0 = \frac{14.1MeV}{\rho\beta}\sqrt{\frac{l}{X_0}}$$

p: momentum
β: velocity
X_0: rad. length
l: material thickness

Scatter muon tomography

STATE OF THE ART – PRESENT STUDIES

- FROM 2000, SEVERAL MUON IMAGING FACILITIES HAD BEEN SETUP ALL OVER THE WORLD BASED ON DIFFERENT TYPES OF DETECTORS, SUCH AS DRIFT TUBE, DRIFT CHAMBER, GEM, RPC, SCINTILLATOR AND SO ON.

LANL FIT AECL BU GU TSINGHUA







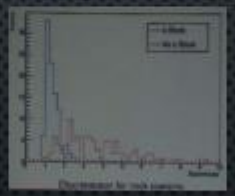
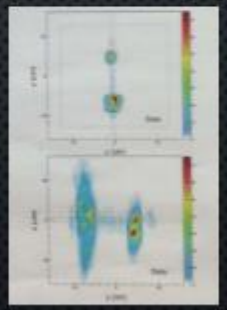
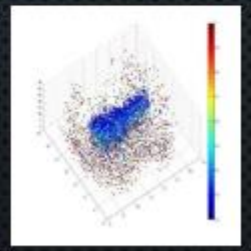

G. Aielli Tuesday, March 25, 2014 9

Courtesy G.Aielli, INFN

Scatter muon tomography + gamma detection

Multi-Mode Passive Detection System (MMPDS)

"MMPDS can scan a typical 40-foot shipping container in 45 seconds, on average"

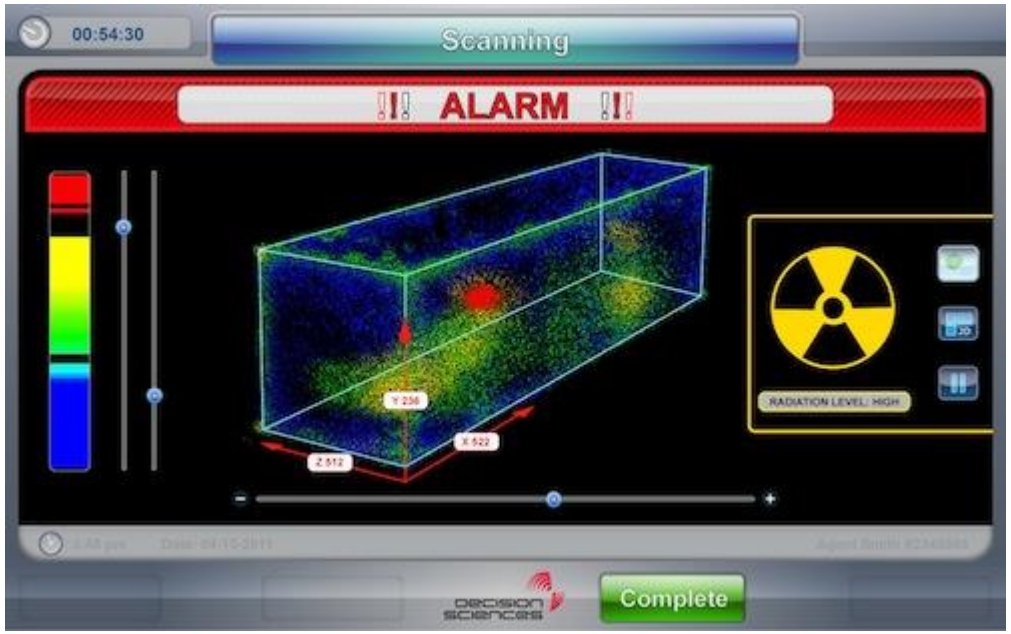

Installed in Freeport, Bahamas

http://www.decisionsciencescorp.com/

Scatter muon tomography – influence of some design parameters

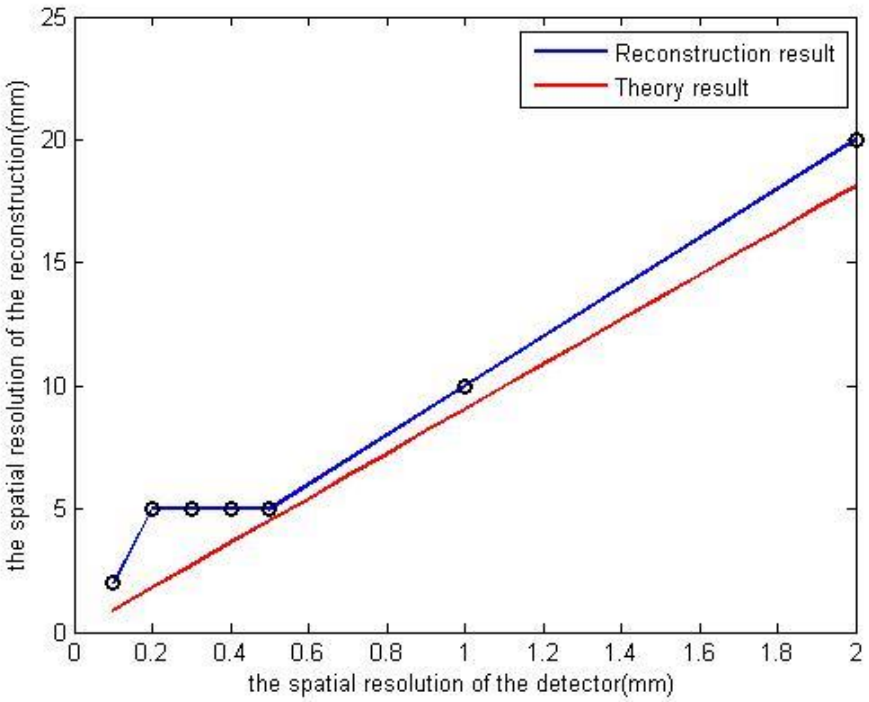

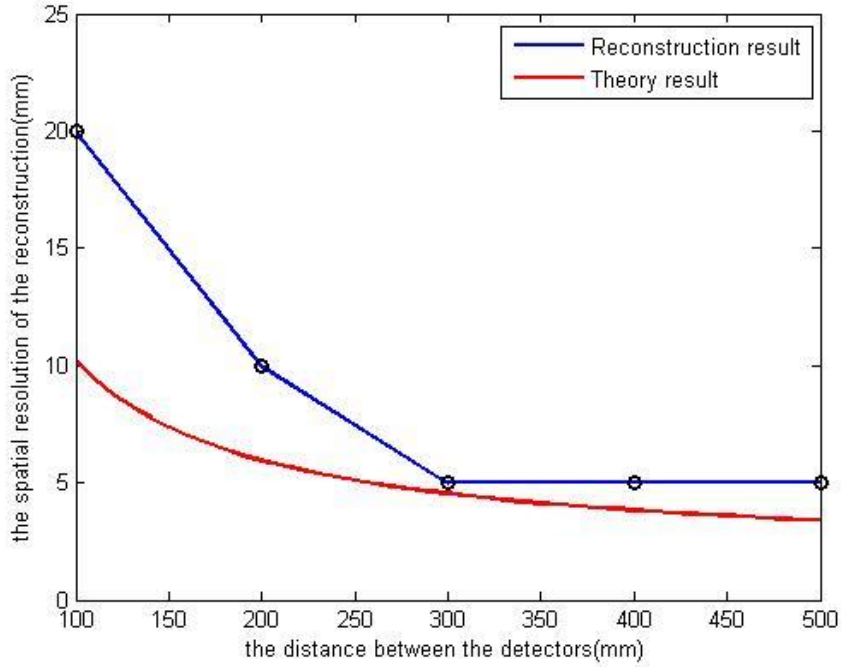

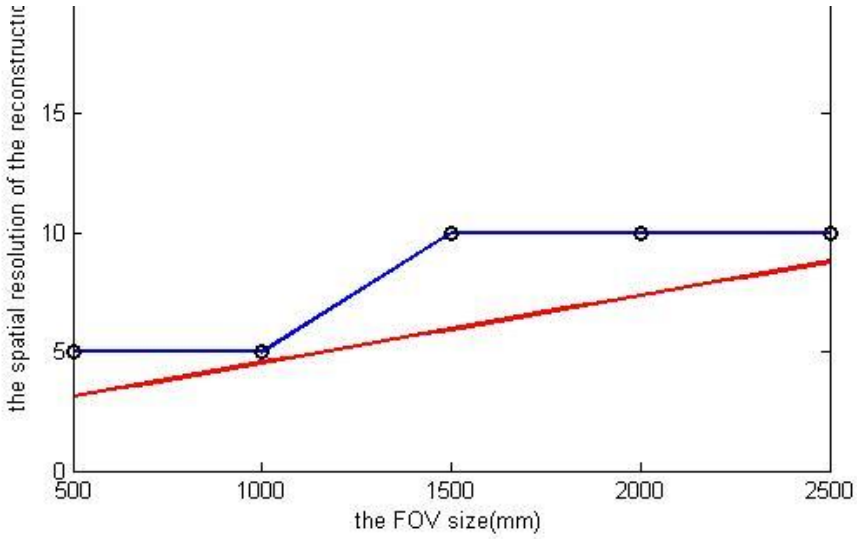

"Preliminary Analysis of the Influence of MRPC Detector Spatial Resolution to the reconstruction spatial resolution in Cosmic-ray Muon Tomography"
B. Yu et al, RPC2014

Scatter muon tomography – yes/no disrimination

Clustering algorithms

- Discriminator value is used as binary classifier, based on a pre-defined threshold.
- Evaluate classifier by comparing true positive and false positive rate on 100 sets of 1 minute simulated cosmics.
- Assuming perfect momentum information, 1 minute of data is enough to reliably identify the block of U in most scenarios.

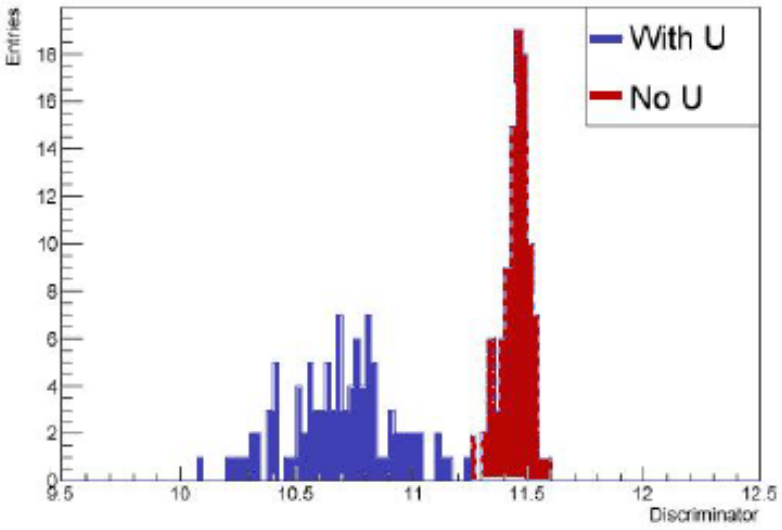

Cargo container with stone

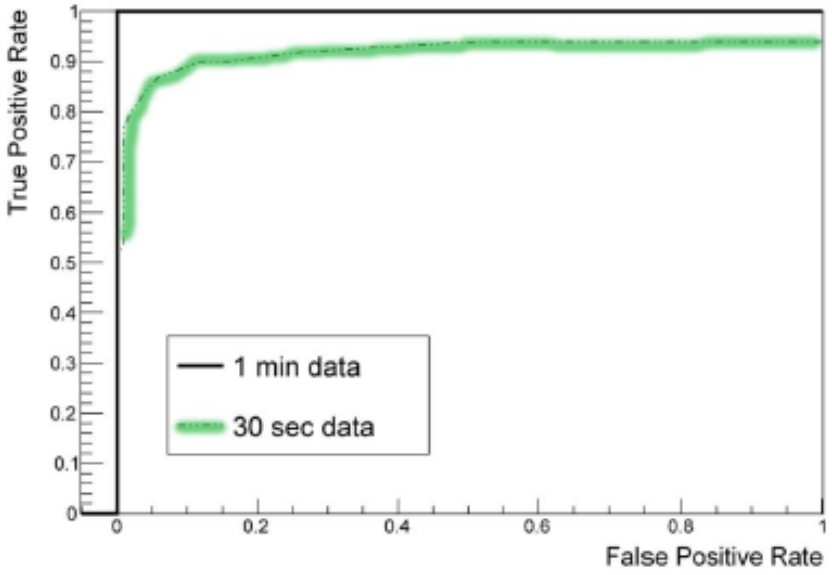

"Toward a RPC-based muon tomography system for cargo containers" P. Baesso et al, RPC2014

State-of-the-art small-animal PET:

- Technique experiences worldwide exponential growth supported e.g. by pharmaceutical industry and biomedical, fundamental science.

Raytest, Germany

Inveon DPET, Siemens

State-of-the-art small-animal PET:

- Technique experiences worldwide exponential growth supported e.g. by pharmaceutical industry and biomedical, fundamental science.

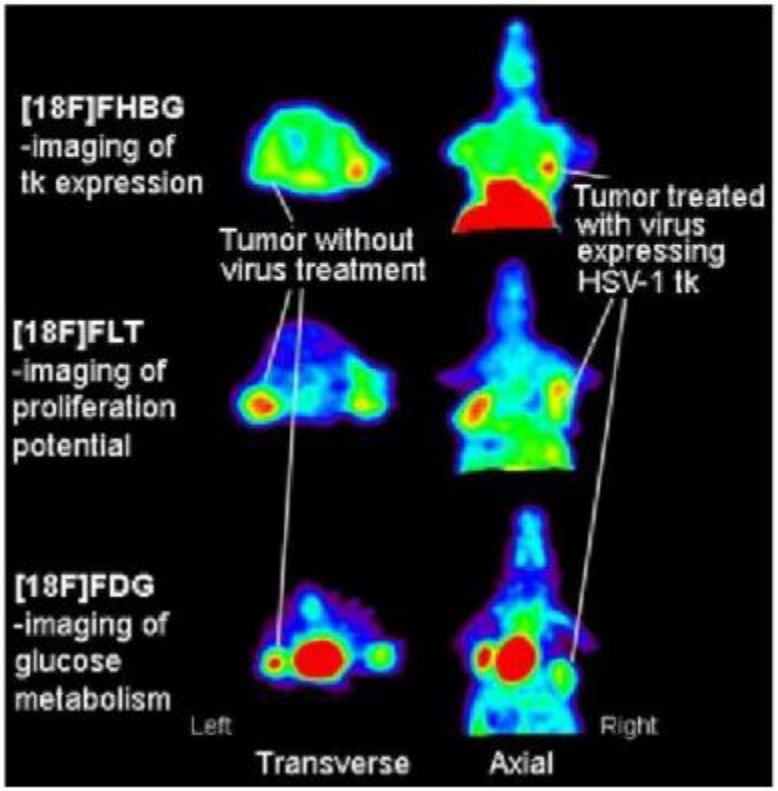

- From Athinoula Martinos Center for Biomedical Imaging
- FHBG = fluoro-hydroxy-metil-butil-guanine.
- HSV-1 = Herpes simplex virus-1.
- FDG = fluoro-desoxy-glucose.
- FLT = desoxy-fluorothymidine.

Rationale is based on state-of-the-art of PET (positron emission tomography):

- Technique experiences growing utilization in nuclear medicine, e.g. for diagnostic/screening/staging of oncologic, neurologic, and cardiac disease.

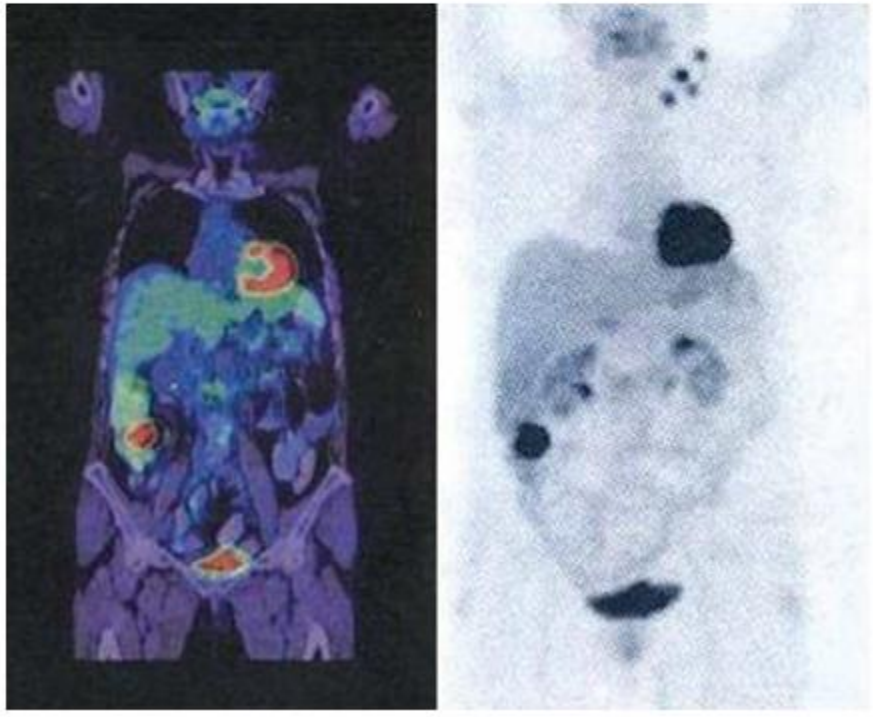

- E.g. Palmisano et al. Saudi J Gastroenterol 2011
- F, 64 a., symptoms: palpable supracavicular, ganglionic adenopathies, asthenia, anorexia.
- PET-based diagnostic: adenocarcinoma of the ascendent colon.

Principles of PET

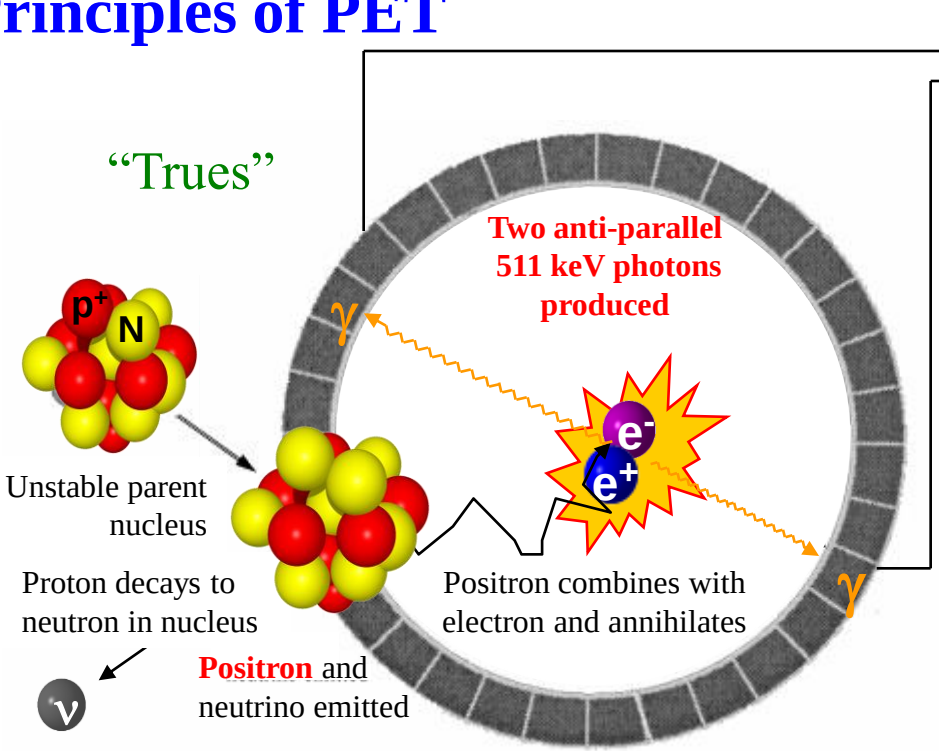

Time coincidence is the main trigger

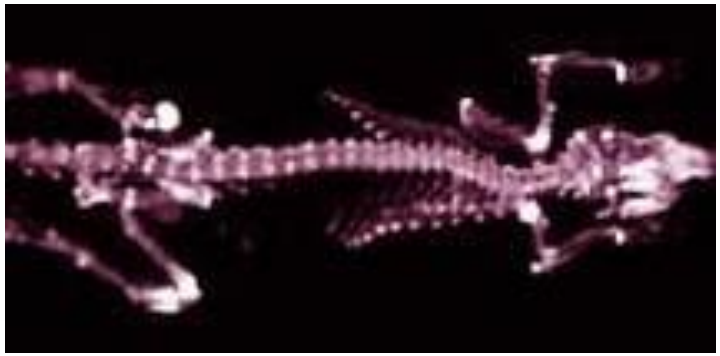

Nice rat image taken with the "HIDAC" scanner (High Density Avalanche Chamber)

Sources of image noise (background): $NEC = \frac{T^2}{T + S + 2R}$

Counting noise

"Randoms"

Avoided by sharper timing

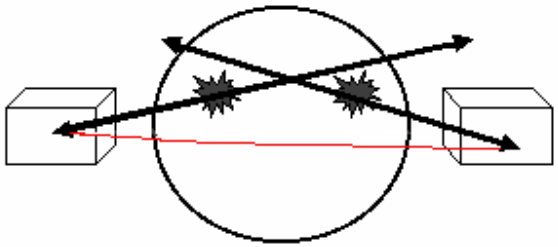

"Scatters"

Avoided by energy discrimination

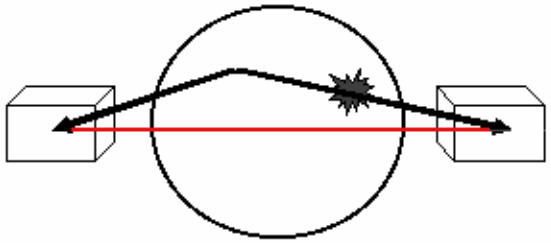

TOF (time-of-flight) - PET

$$TOF\ sensitivity\ advantage \approx \frac{object\ size}{(c/2)\ time\ resolution}$$

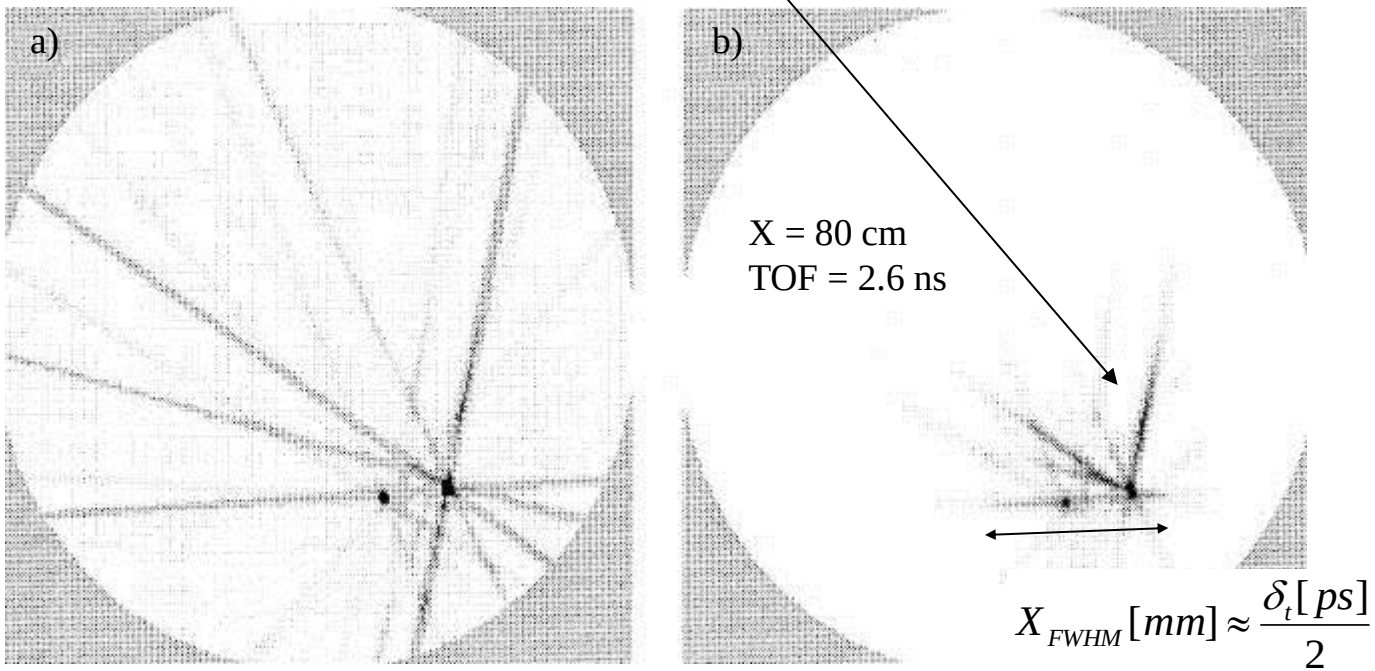

a) Reconstructed image without TOF.
b) Reconstructed image using TOF information

[NIM A 471(2001) 200-204]

The importance of high sensitivity in PET

$$\text{Image quality} \propto \text{counts/pixel}$$

$$\text{counts/pixel} \propto \frac{\text{activity injected in patient} \times \text{measurement time}}{\text{number of pixels}} \times \text{sensitivity}$$

Lower the injected dose
⇒ PET exam can be used on lower risk patients

Higher resolution possible
⇒ Smaller tumours visible

More examinations per unit time
⇒ Lower examination costs
⇒ More people can afford PET exams

Lives saved through earlier cancer detection?

Single-bed full-body human PET

Standard PET

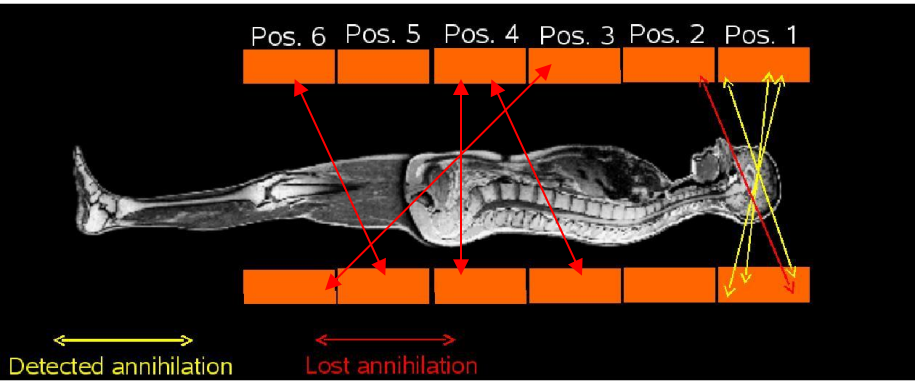

Most photons are lost

Made with crystal "blocks" 5x5 cm

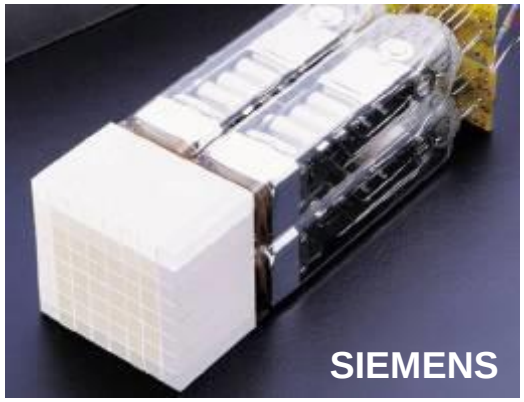

Comercial value=1.5M€

Whole-body FOV PET

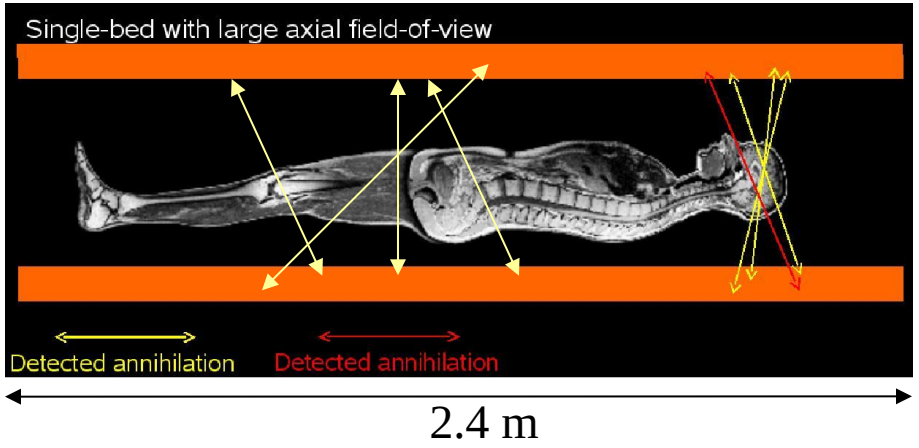

Most photons have a chance to be seen

Extremely expensive if based on crystals
⇒ RPC-PET

The concept was independently reviewed by mainstream workers and found worth pursuing.

[L.Erickson et al, 2008 IEEE MIC]

[D.B.Crosetto 2000 IEEE NSS]

The basic idea for RPC-based TOF-PET

The converter-plate principle

Use the electrode plates as a γ converter, taking advantage of the natural layered construction of the RPCs.

[Blanco et al, 2002]

Stacked RPCs

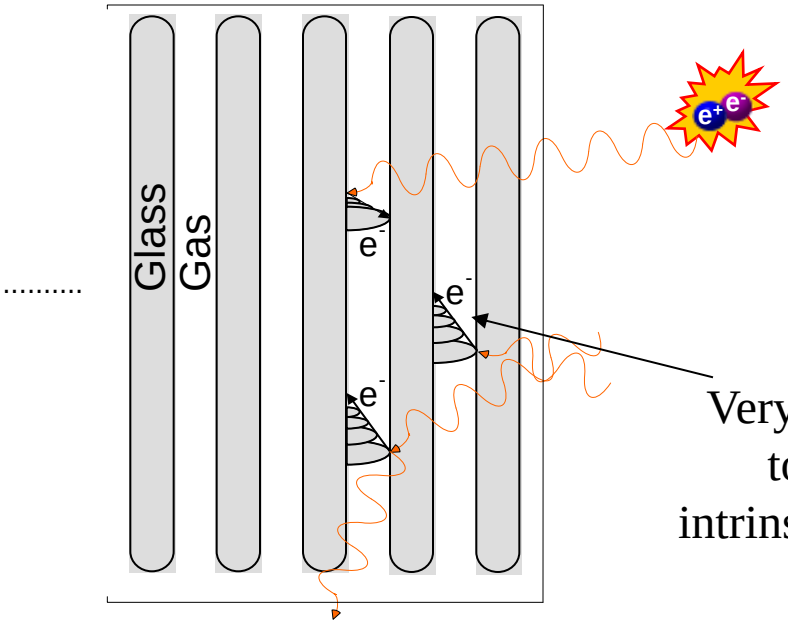

Time resolution for 511 keV photons:
(our routine lab-test tool)

90 ps σ for 1 photon

300 ps FWHM for the photon pair

Very small gas gap
to minimize
intrinsic internal error

A previous work on PET with gaseous detectors (21 lead plates + 20 MWPCs = 7% efficiency)

"The Rutherford Appleton Laboratory´s Mark I Multiwire Proportional Counter Positron Camera"
J.E. Bateman et al. NIM 225 (1984) 209-231

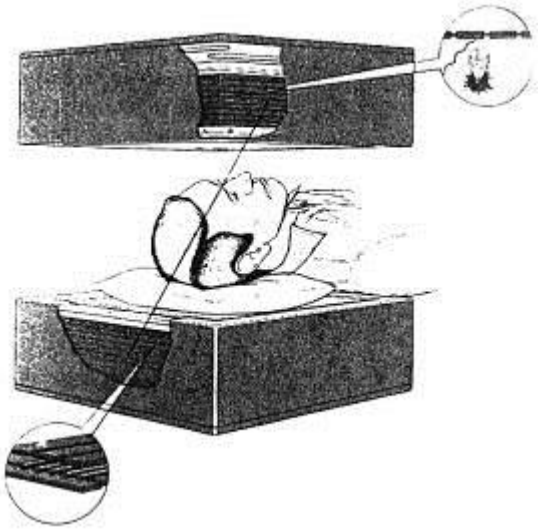

Comparison with GEANT - efficiency

Optimum efficiency is balanced by beam absorption (thicker plates) and extraction probability (thinner plates)

Optimum thickness depends on the number of plates and on the material.

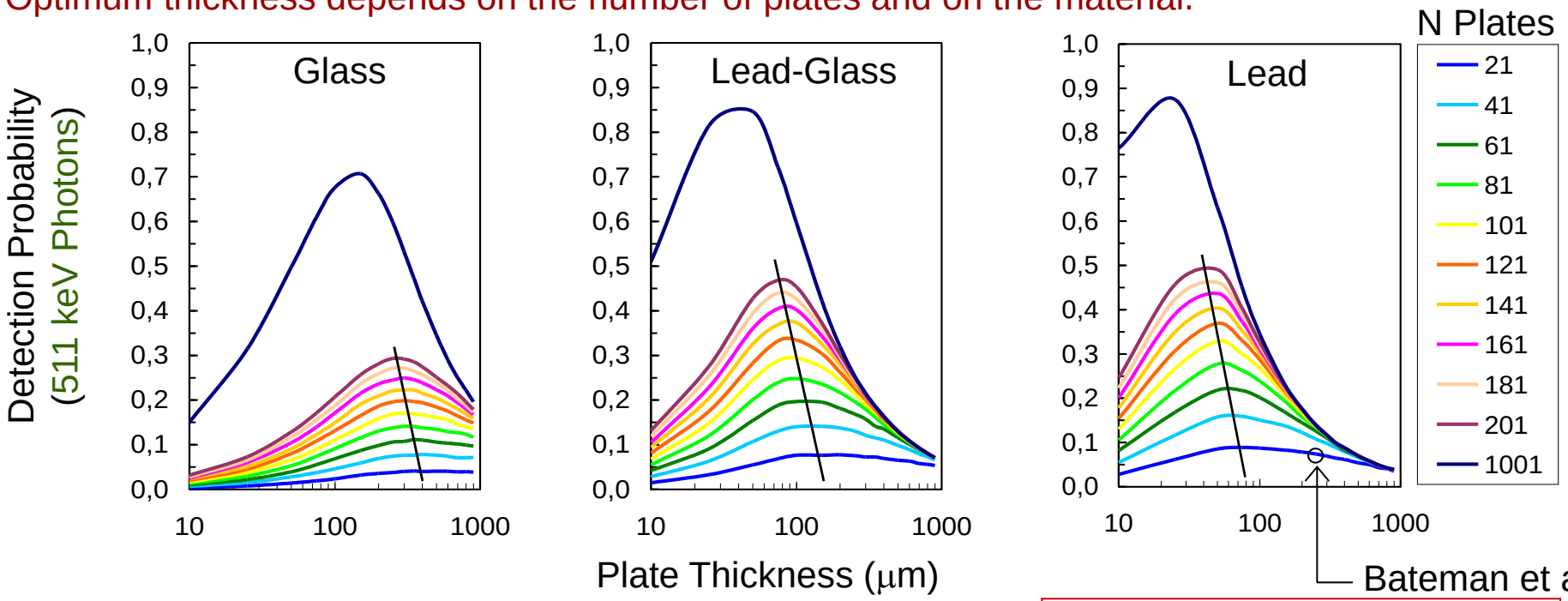

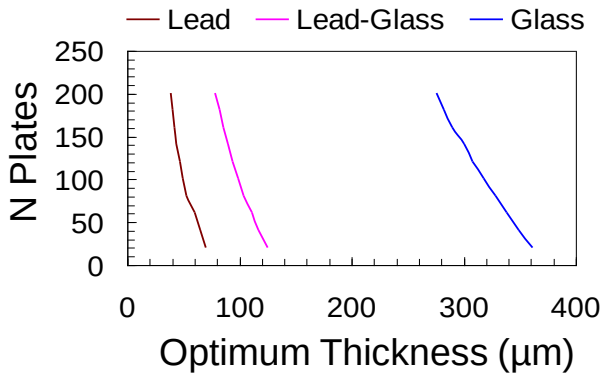

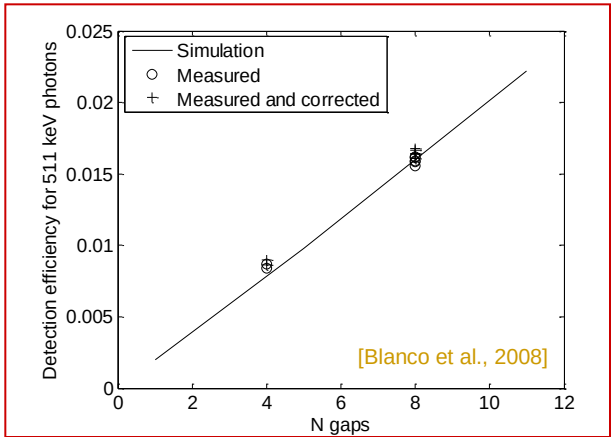

GEANT - energy dependence

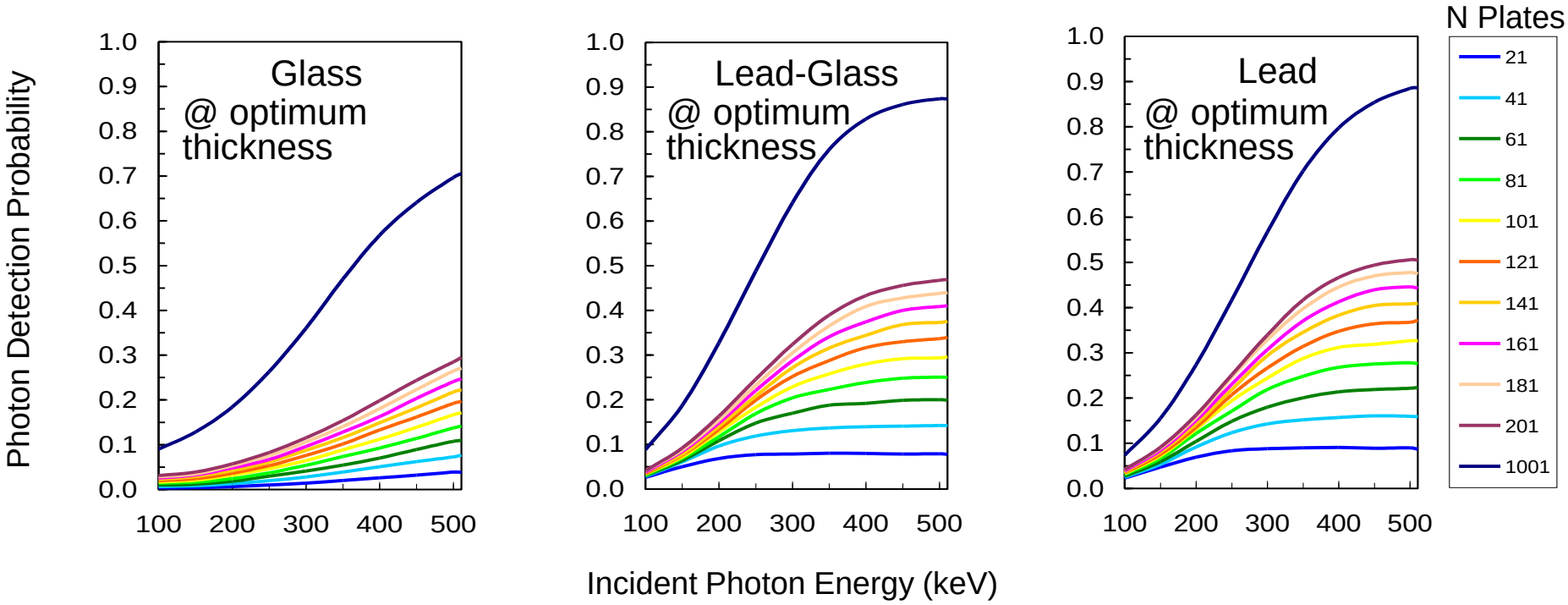

Strong ENERGY SENSITIVY
scattered photons statistically rejected

		Material		
	ε_{max}	Glass	Lead-Glass	Lead
N Plates	101	*17%*	*29%*	*31%*
	201	*29%*	*47%*	*50%*

Comparison with the standard PET technology

Disadvantages

Certainly a much smaller efficiency: 20 to 50% as compared to 70 to 80%.
No energy resolution, but there is an equivalent energy sensitivity... more later.
Detector scatter (vs. "misidentified fraction" in crystal blocks)

Possible specialized PET applications

Advantages

Increasing system sensitivity

Inexpensive ⇒ large areas possible ⇒ large solid angle coverage
Excelent timing ⇒ TOF-PET possible+optimum randoms rejection

} Whole-body Human PET

Increasing position accuracy

Gaseous detectors routinely deliver 0.1 mm resolution
Full 3D localization possible ⇒ no gross parallax error
The very small gap minimizes intrinsic errors

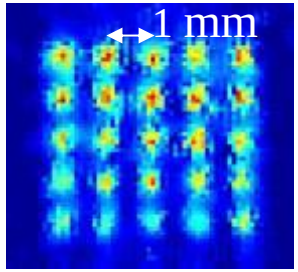

} Small Animal PET

Simulation: 0.51mm FWHM

Other

Simultaneous full body imaging (continuous uptake signal)
Compatible with magnetic field ⇒ PET-MRI can be considered

Small animal PET - a first prototype

Aimed at **verifying** the concept and show the **viability** of a **sub-millimetric spatial resolution**.

16 stacked RPCs

Charge-sensitive electronics allowing interstrip position interpolation

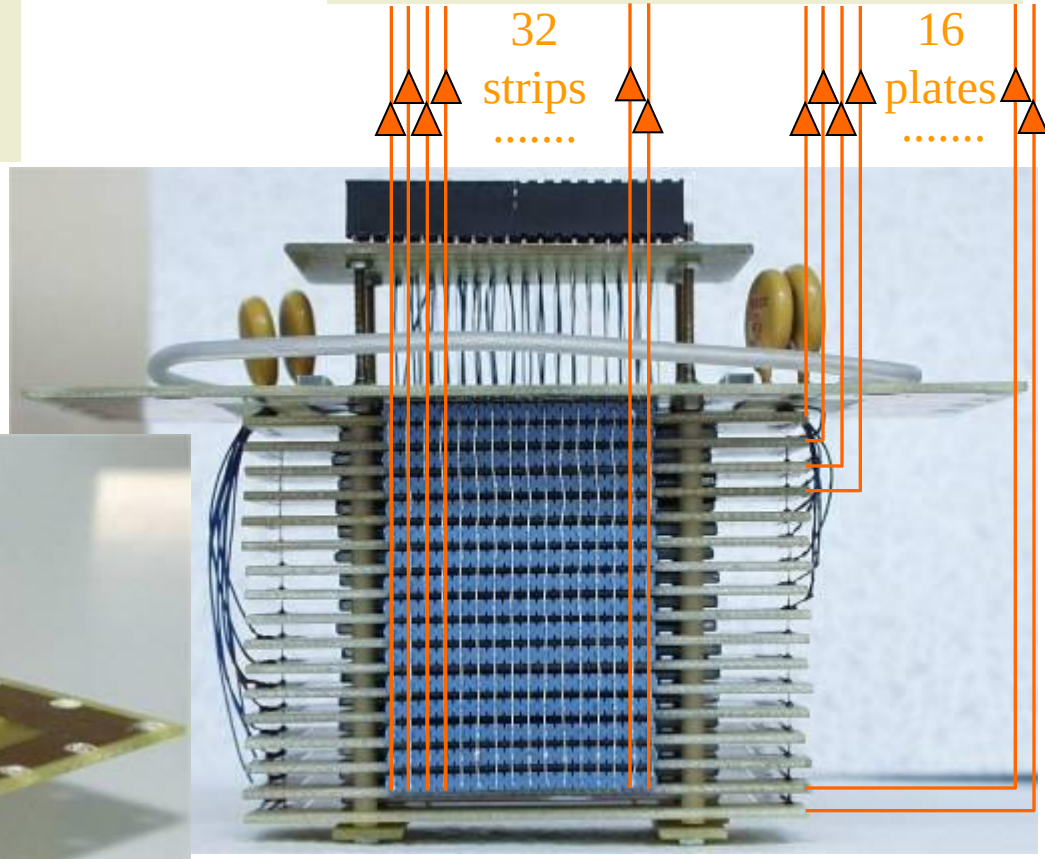

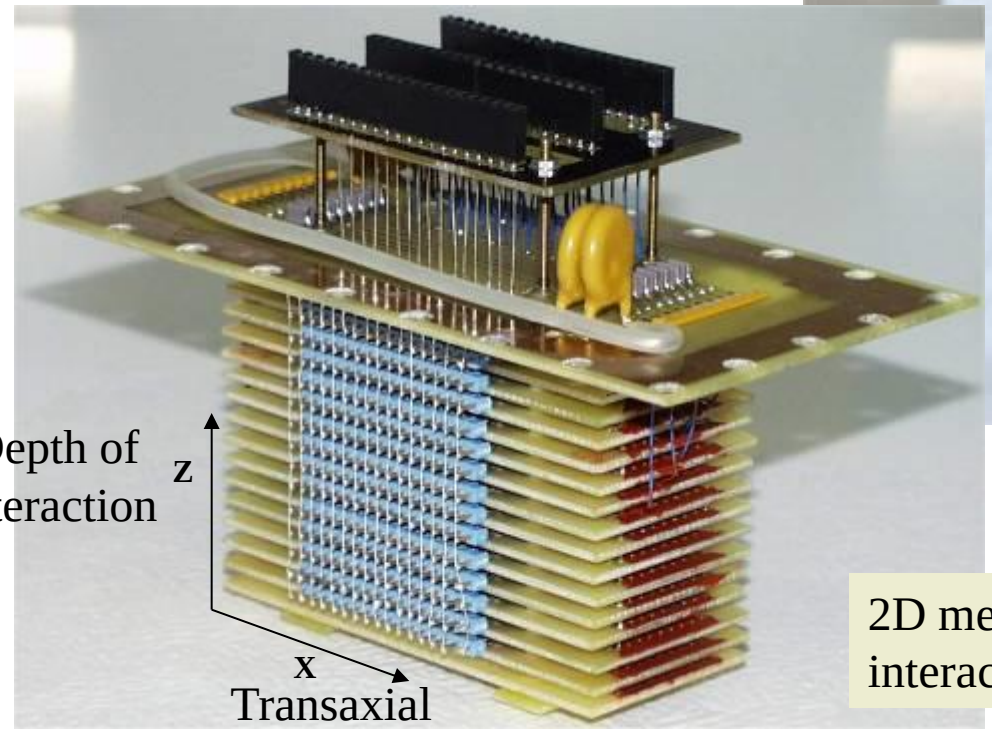

2D measurement of the photon interaction point

System

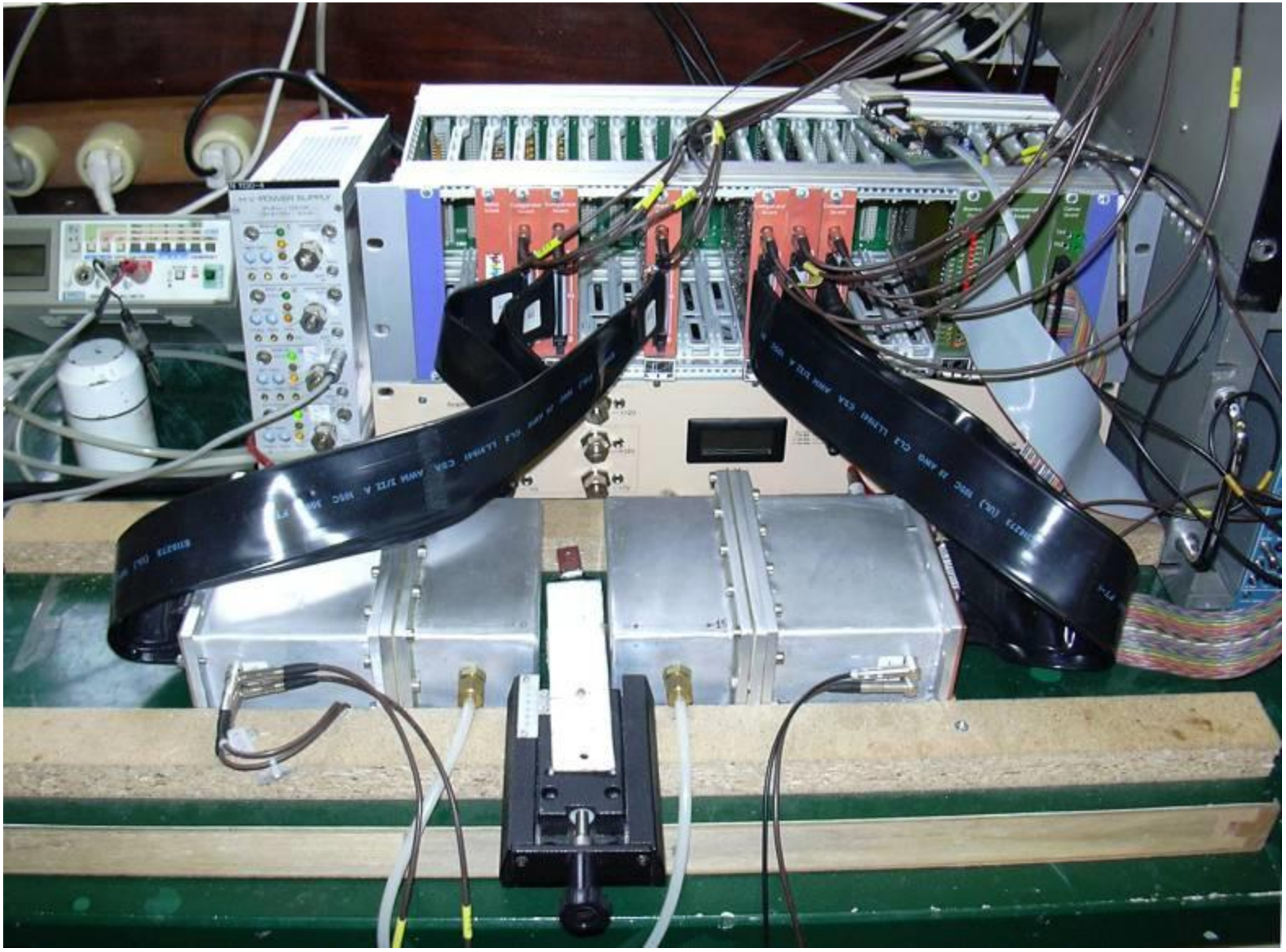

Intrinsic spatial resolution

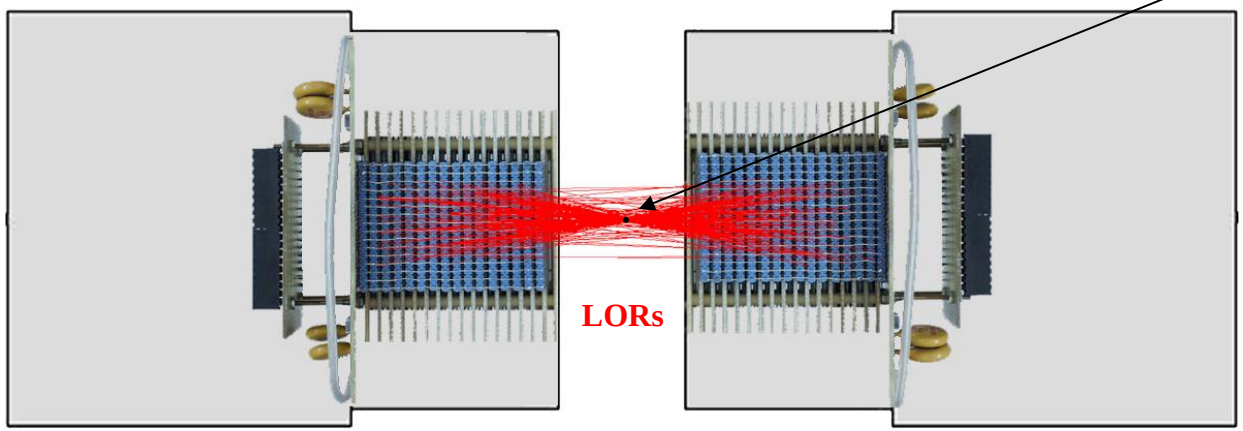

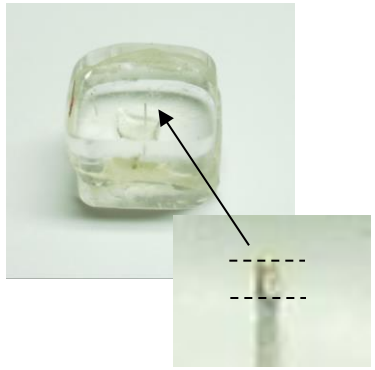

Custom-made
^{22}Na source

0.22 Ø x 0.5 mm

Red lines correspond to real data acquired with the ^{22}Na source

LOR = Line of Response. Connects the interaction points of the photons.

D = Distance between each LOR and the center of the system

Image spatial resolution (gaussian fitting)

Filtered Back Projection FBP

~ 465 μm FWHM

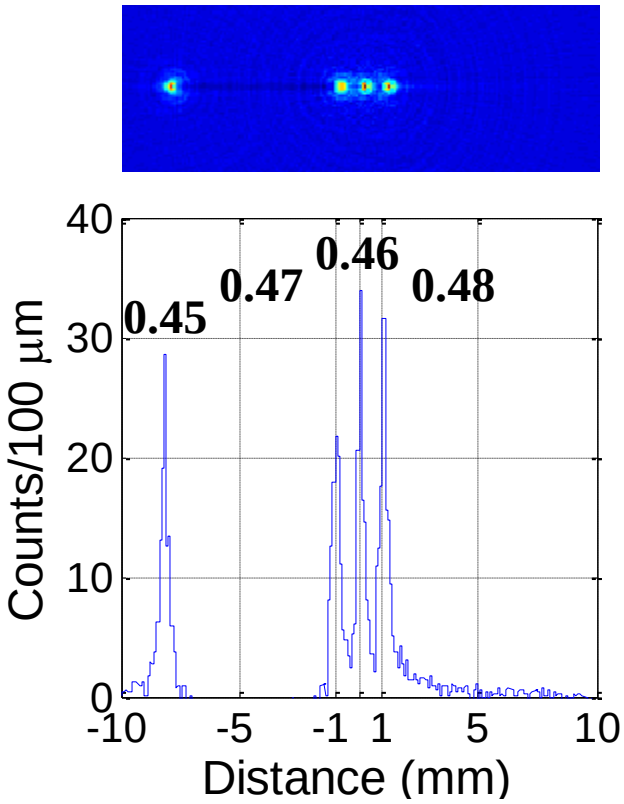

Maximum likelihood-expectation maximization with resolution modeling (ML-EM)

~ 305 μm FWHM

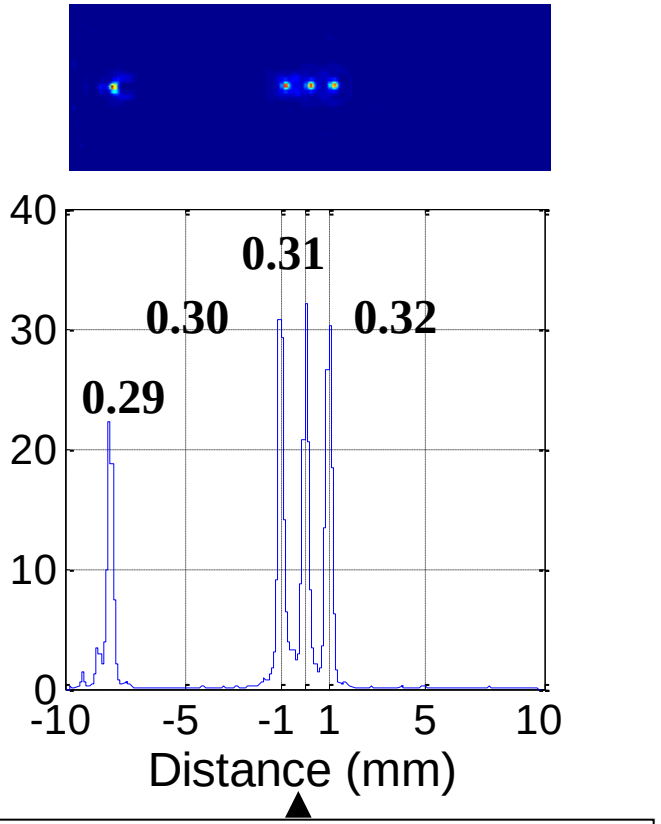

[Blanco, IEEE MIC 2004]

Proceeding IEEE MIC (2004) M2-177

Homogeneous spatial resolution over the entire field-of-view

Simulated count rate performance

Evaluation of the count rate performance Prompts, Randoms, and NECR

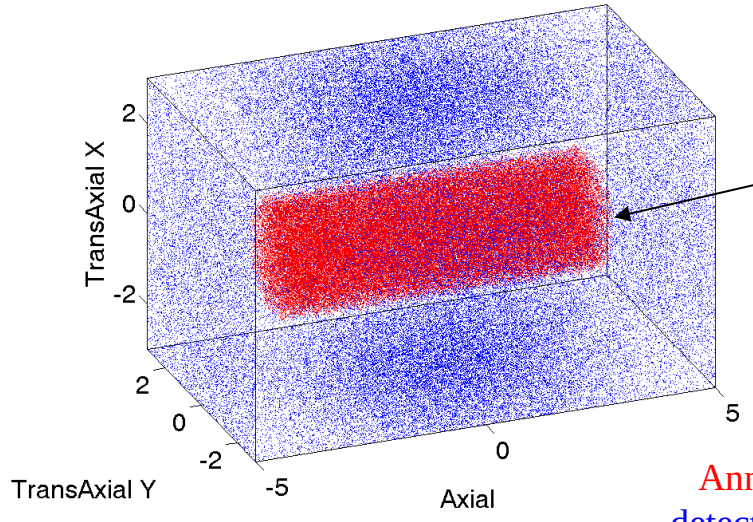

Mouse size phantom:

25 Ø x 70 mm (34 cm^3)

Annihilations and photons on the detector surface from the simulation.

GEANT4

Characteristic of the simulated system:

- **90% Solid angle coverage** => defining a FOV of 60 Ø x 100 mm axial.
- Narrow **coincidence window 1 ns. (Timing resolution 300 ps FWHM)**
- **Dead time ~ 100 ns.**
- **10% - 15% detection efficiency.**

[Blanco, IEEE MIC 2004]

Comparison small animal PET scanners

System	Detector	FOV Trans / Axial ⌀(mm) /(mm)	Δt /τ_{cw} (ns)*	Energy resolution(%) @511keV	CFOV and off-centre Spatial Resolution (mm) FWHM[0]	ACS (%) (E_w (keV))	Peak NEC (kcps)@ activity (MBq)	Apprx Price k€[1]
Inveon®	LSO	100 / 127	/ 3.4	18	$1.5-1.5-1.2$[4] $1.7-2.2-1.5$[4]	5.7 (350 – 650)[5] 7.4 (250 – 750)[5]	538@131[2,6] 1734@147[3,6]	650
Mosaic®	GSO	120 / 128	/ 12	17	$2.7-2.8-3.4$[7] $2.8-2.9-4.1$[7]	1.1 (410 – 665)	129@101[2,8] 308@83[3,8]	600
eXplore VISTA®	$LYSO$ $-GSO$	67 / 48	1.3 / 5.0	∼ 30	$1.4-1.4-1.4$[9] $2.1-1.4-2.1$[9]	2.2 (400 – 700)[10] 6.5 (100 – 700)[10]	91@35.8[2] 170@22.6[3]	700
NanoPET®	$LYSO$	94 / 95	/	–	< 1.2[11] – –	8.3 (250 – 750)	720[3]	––
Raytest ClearPET®	$LYSO$ $-LuYAP$	135 / 110	2.0 / 12	∼ 20	$1.5-1.1-$ [12] $2.0-1.5-$ [12]	2.1 (350 – 650)[13] 3.5 (250 – 750)[13]	73@18[2]	––
LabPET12®	$LYSO$ $-LGSO$	100 / 75	6.6 / 13	∼ 20	$1.4-1.3-1.4$[14] $2.1-2.0-$ [14]	2.1 (250 – 650)	121@168[2,15] 252@131[3,15]	––
HIDAC	$MWPC$	170 / 280	/ 40	/[16]	1.1[17] 1.1[17]	1.5 (–)[18] 1.5 (–)[18]	52@26[2] 67@23[3]	500
RPC-PET	RPC	60 / 100	0.3 / 1.0	/[19]	$0.43-0.43-$ [20] $0.43-0.43-$ [20]	2.1 (–)[21] 2.1 (–)[21]	320@88[3,22]	100[23]

Table 7.1: Comparison of the main characteristics of an RPC-PET system with preclinical PET systems.

ACS Absolute Central point source Sensitivity

·* Δt and τ_{cw} are the timing resolution and time coincidence window in ns.
·[0] Radial, tangential and axial spatial resolution. First and second row are resolutions at centre of FOV (CFOV) and off-centre respectively.
·[1] [Shehad et al., 2006]
·[2] Rat-like phanton, [3] Mouse-like phanton.
·[4] $E_w = 350 - 650$ keV, $\tau_{cw} = 3.4$ ns. Reconstructed with FORE and FBP. 20 mm radial offset. [5] $\tau_{cw} = 3.4$ ns. Background subtracted, without scatter or random correction. [6] $E_w = 350 - 650$ keV, random coincidences measured with a delayed window, no normalization and corrections for dead time, scatter or attenuation.
·[7] Reconstructed with FORE and FBP. 20 mm radial offset. [8] Random coincidences measured with a delayed window.
·[9] $E_w = 250 - 700$ keV, reconstructed with FORE and FBP without scatter or attenuation correction. 20 mm radial offset. [10] Without scatter or attenuation correction.
·[11] Reconstructed with FBP.
·[12] $E_w = 250 - 750$ keV, $\tau_{cw} = 20$ ns, 20 mm radial offset. [13] Corrected for random coincidences and Lu natural radioactivity.
·[14] $E_w = 375 - 650$ keV, reconstructed with FBP. [15] $E_w = 250 - 650$ keV.
·[16] Energy is not measured. [17] For all three components and uniform within the entire FOV, reconstructed with FBP. [18] Corrected for scatter coincidences.
·[19] Energy is not measured. [20] Reconstructed with FBP. Axial not measured but should be uniform within the entire FOV for all three components. [21] Simulated, 15% RPC detecion efficiency. [22] Simulated. [23] Estimated.

[Blanco, PhD thesys 2012]

Full scanner for mice

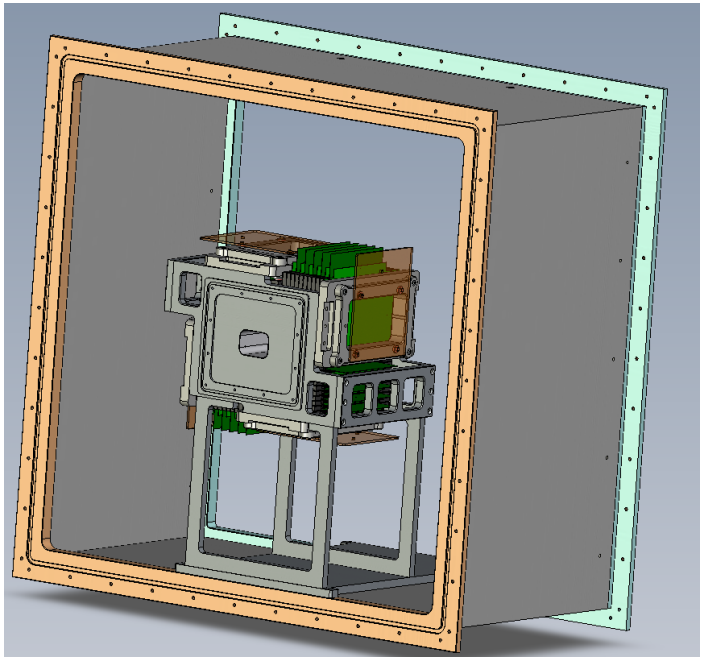

Expected quantum efficiency and resolution

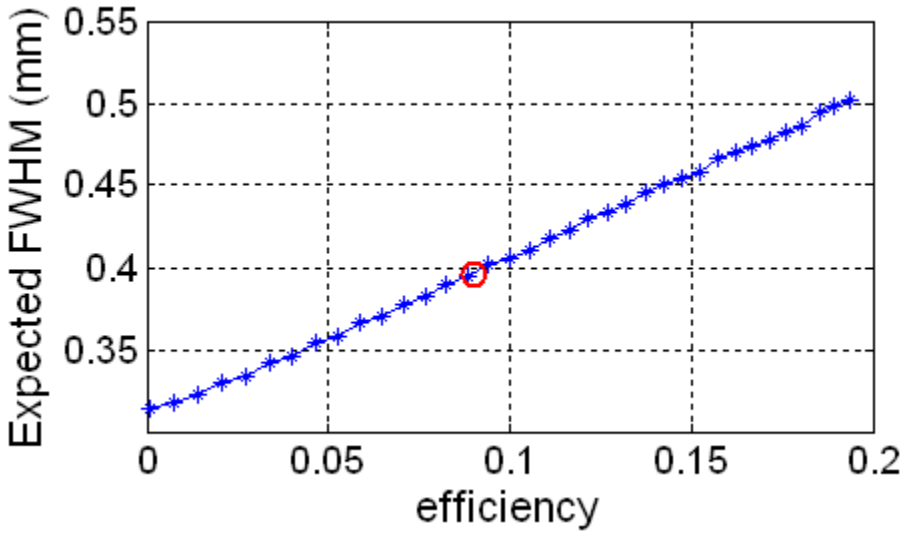

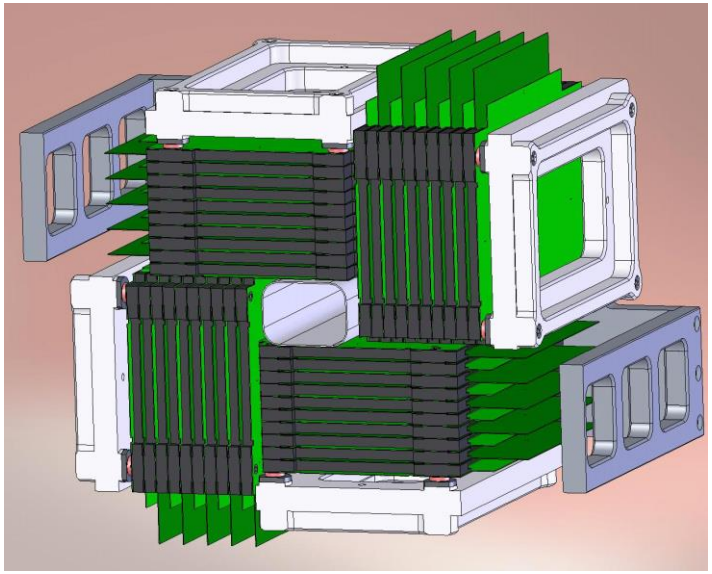

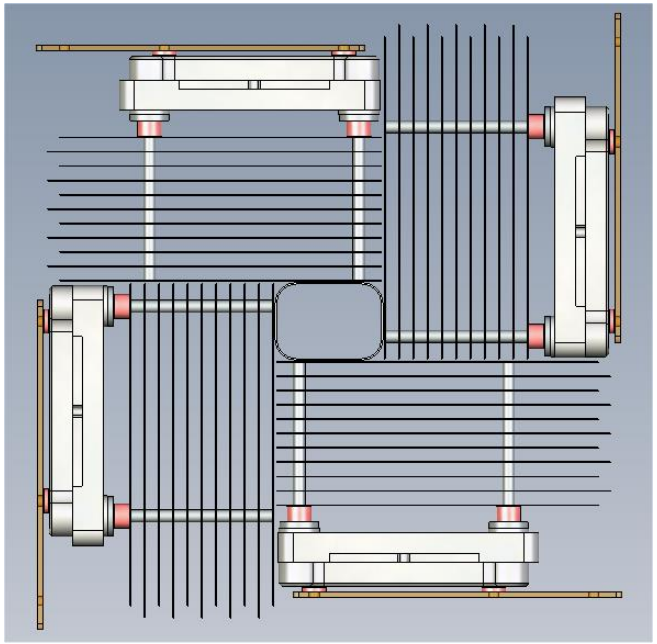

Full scanner for mice (almost finished)

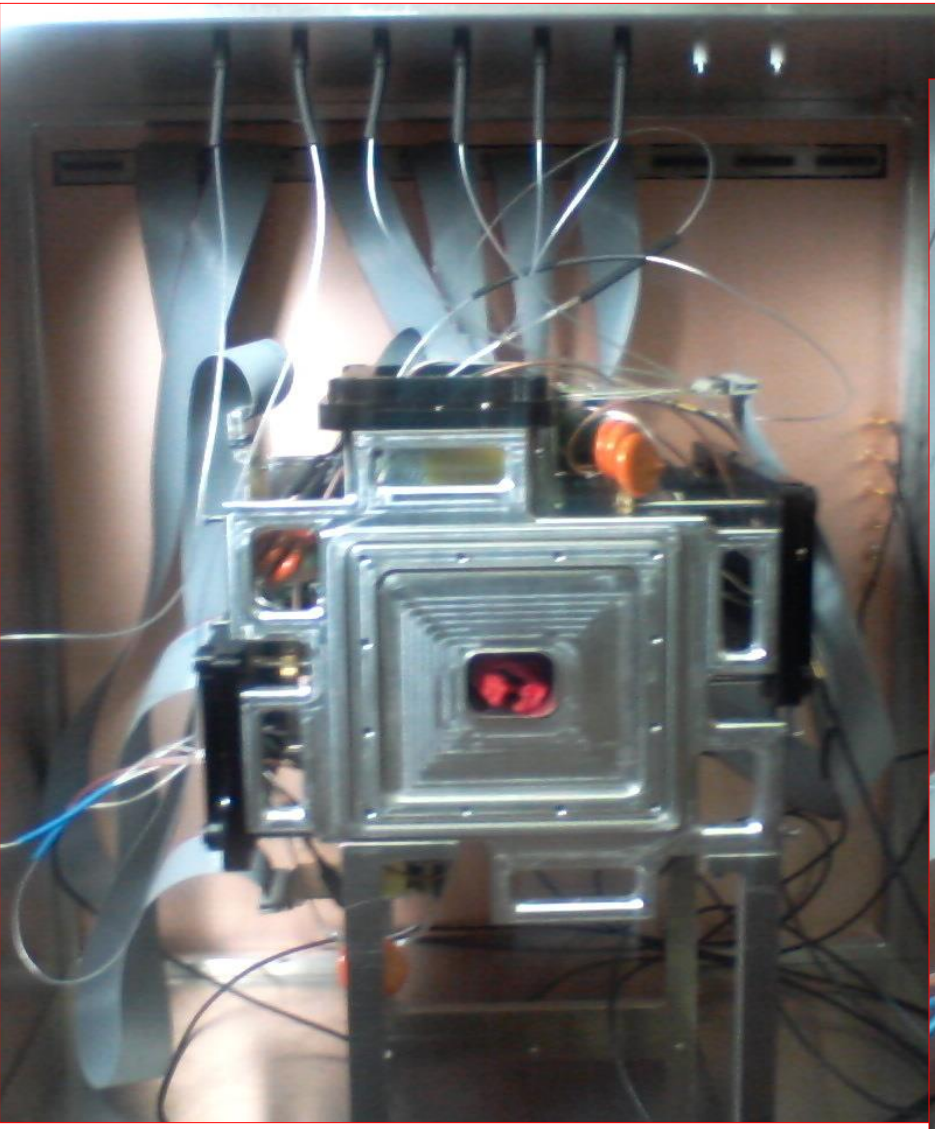

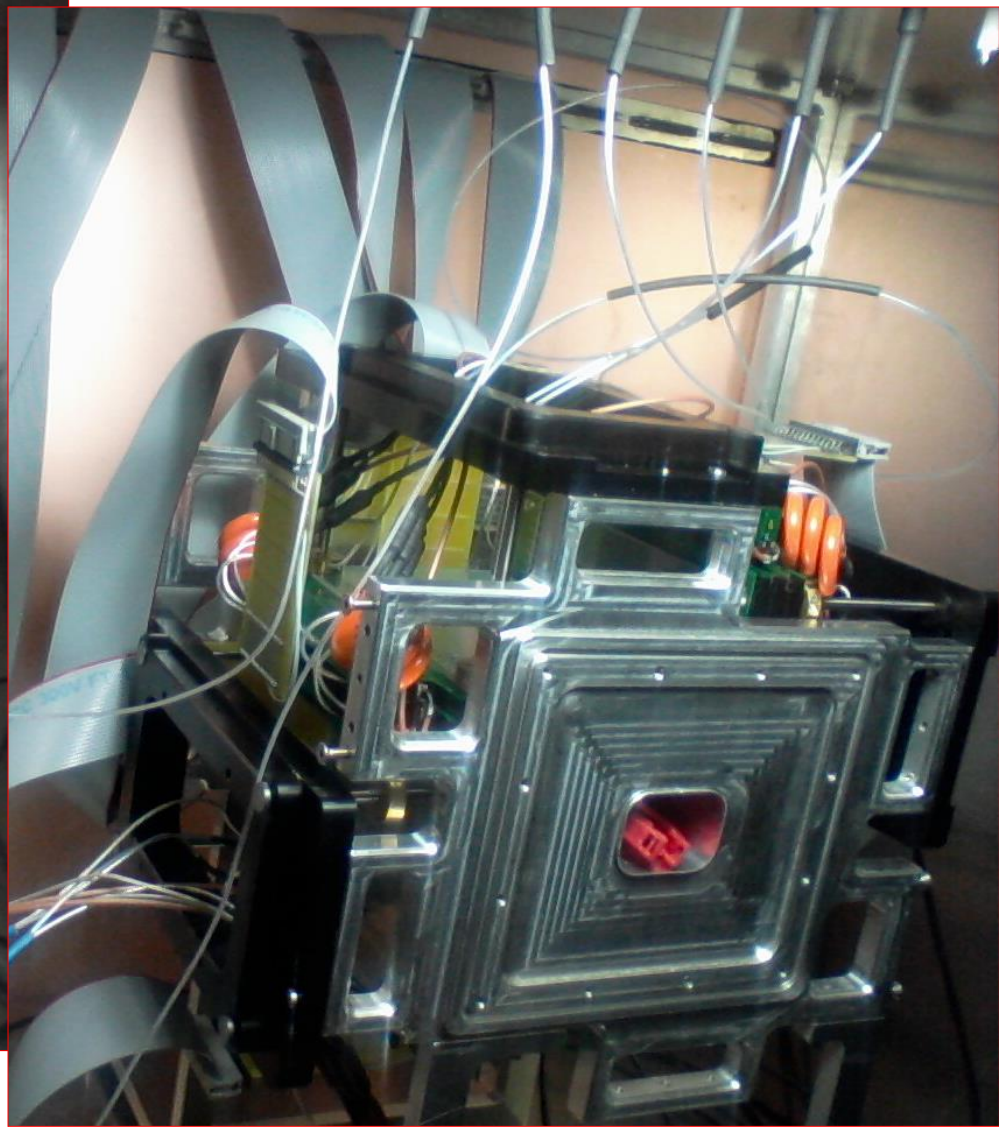

Detector & readout

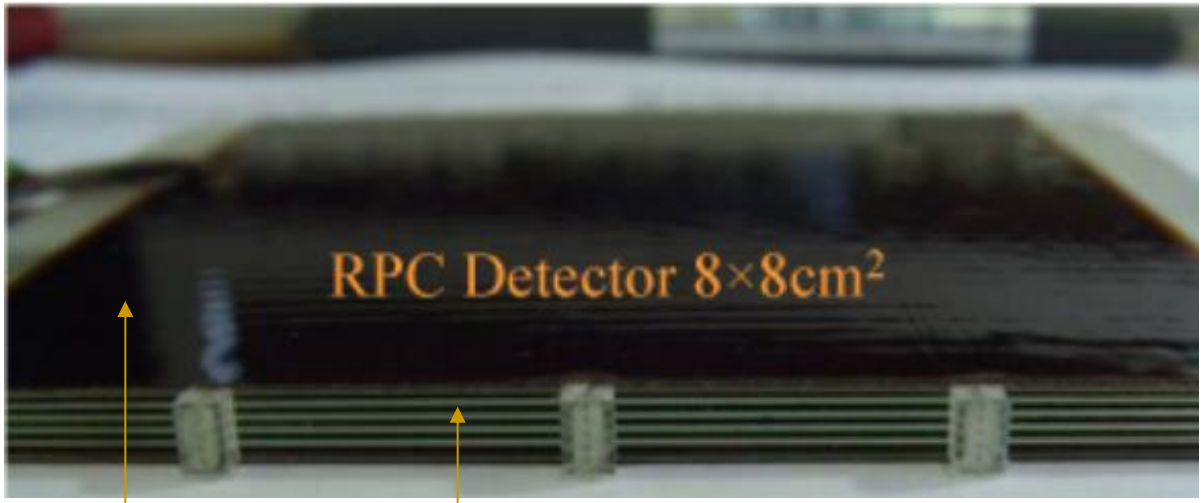

HV distribution layer
(signal-transparent)
kapton insulation

5 gaps 0.35 mm
6 x 0.38mm glass
~5 mm thick

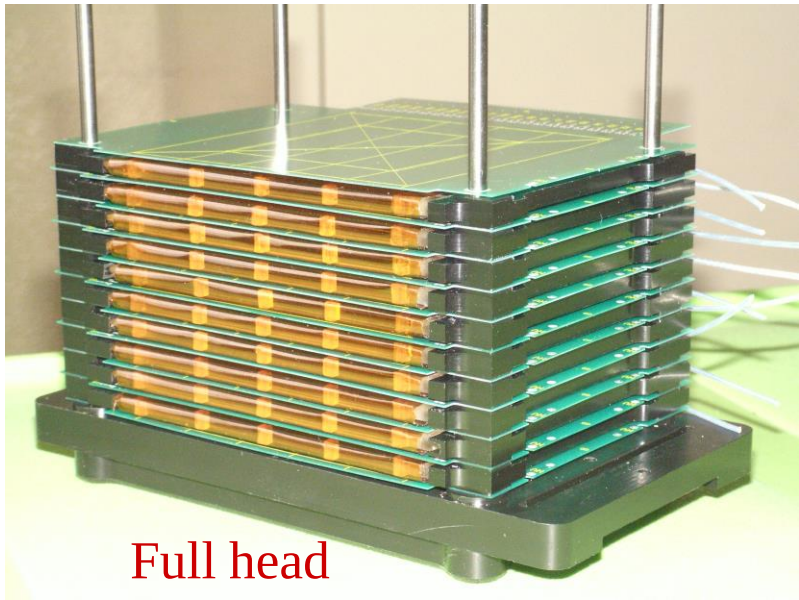

Full head

Readout (meant for accuracy)

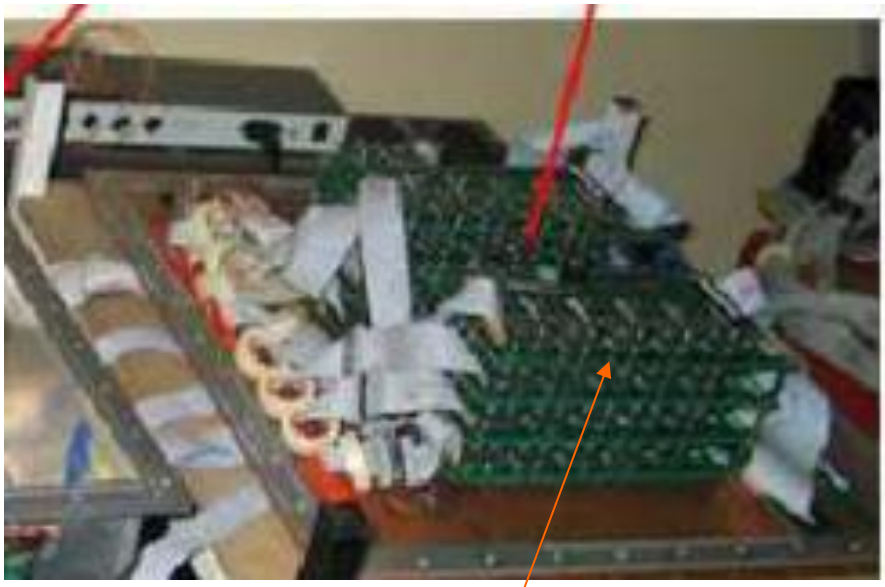

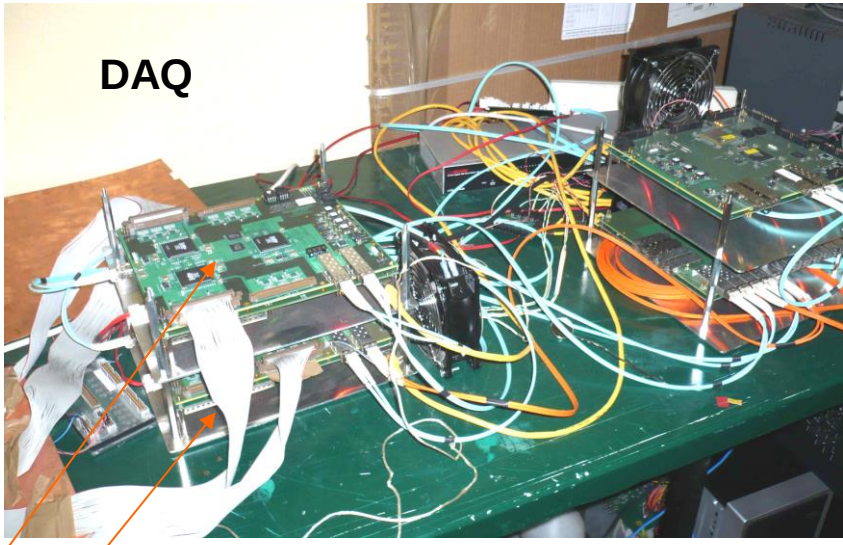

192 charge amplifiers optimized for large Cin
192 channels 12 bit streaming ADC
Digital Pulse Processing by software
Few channels of 100ps TDC also used

Provided by the HADES DAQ group
GSI, IKF (Germany) and JU (Poland).

Not so much hardware ⇒ low cost

Resolution tests in simplified geometry

Two detectors with XY localization

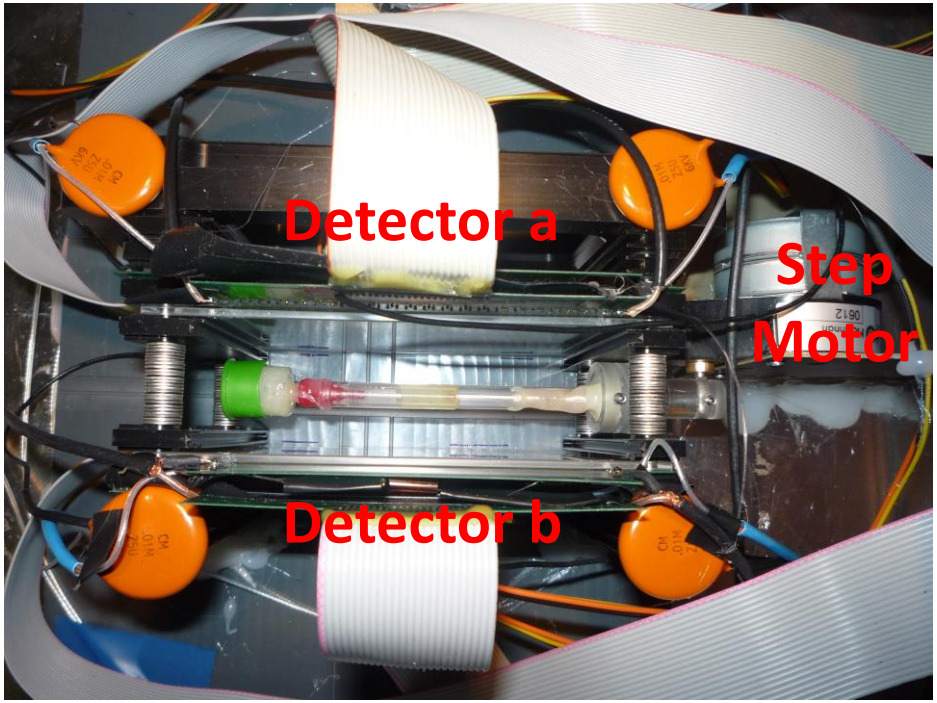

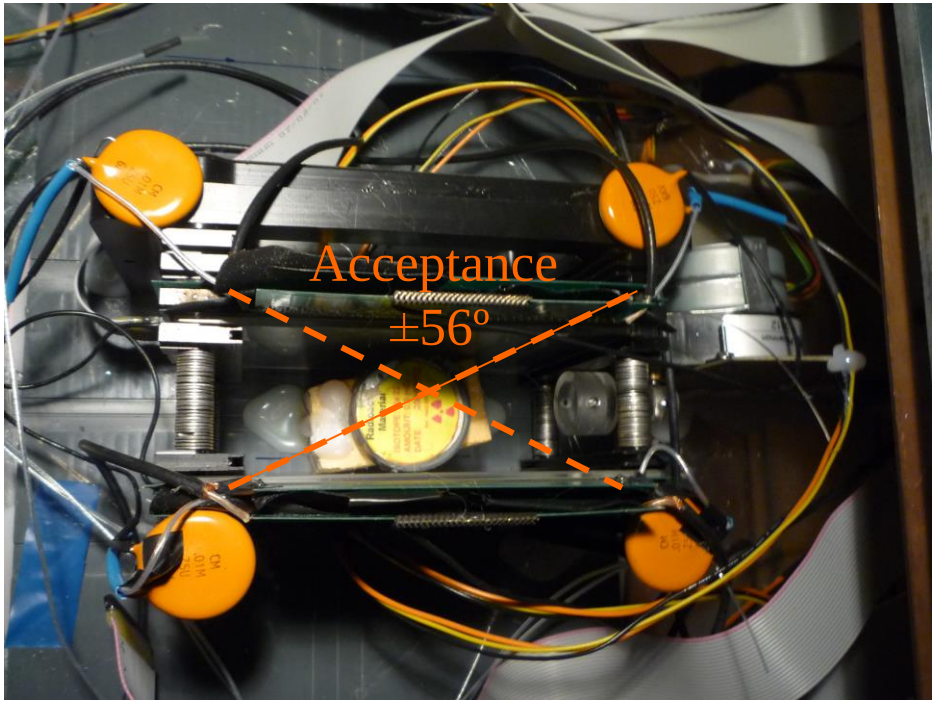

Needle source, 0.2 mm ∅ int.

Planar (disk) source

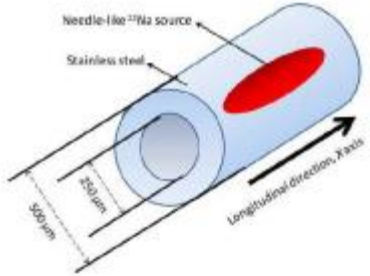

Resolution tests (needle source)

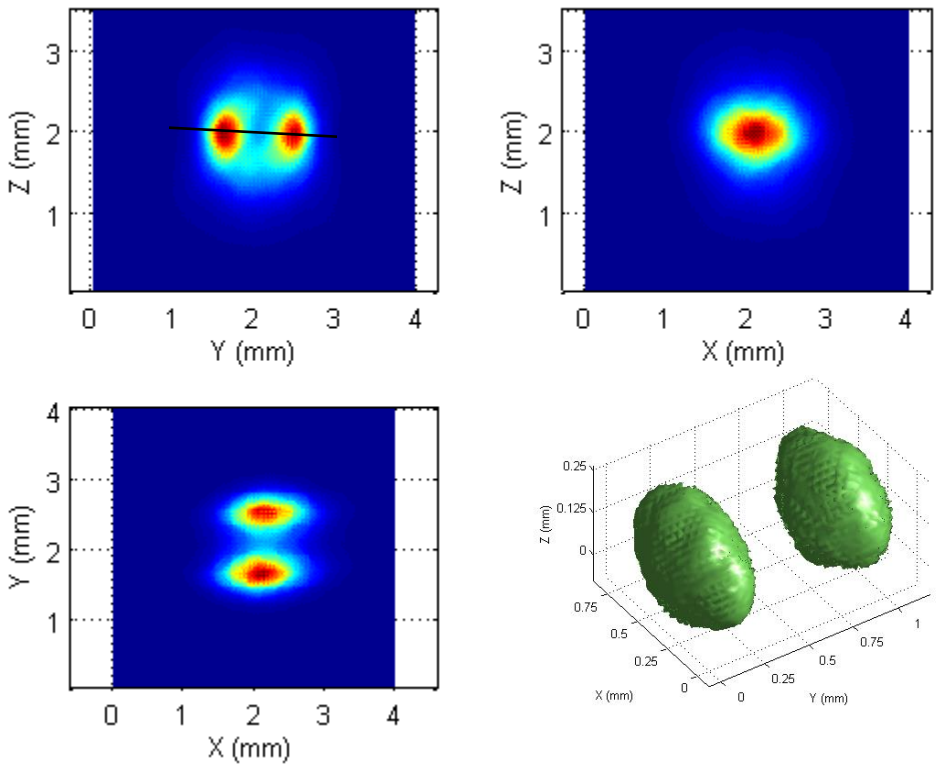

Full area, all angles (up to 56º), all gaps (DOI) MLEM reconstruction

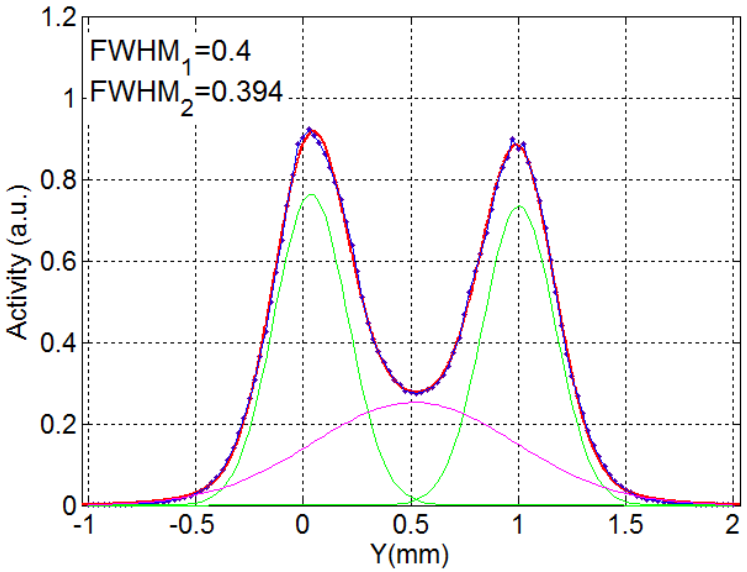

Joint reconstruction of the source in 2 positions separated by 1mm.
~130k LORs in 3.5M 25μm voxels.
Color maps: planar profiles including peak density point.
Isosufaces: 50% rel. activity

Reconstructed activity profile across the black line shown in the upper left panel.
Resolution **~0.4mm FWHM +background**
(Note: source is 0.2mm diam.)

Resolution tests (planar source)

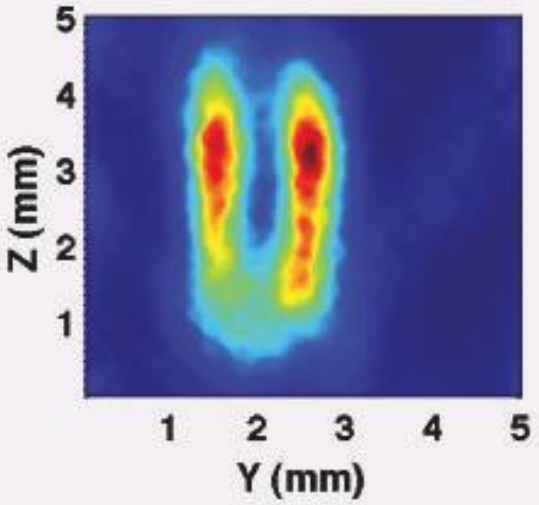

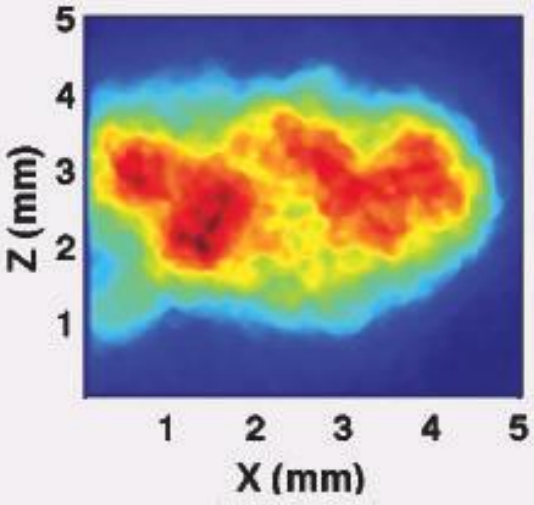

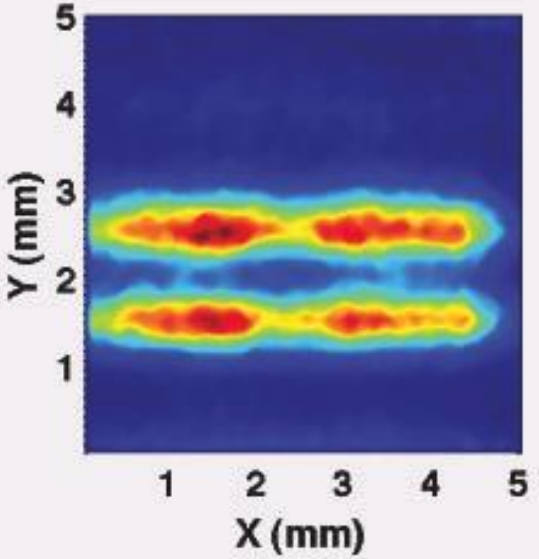

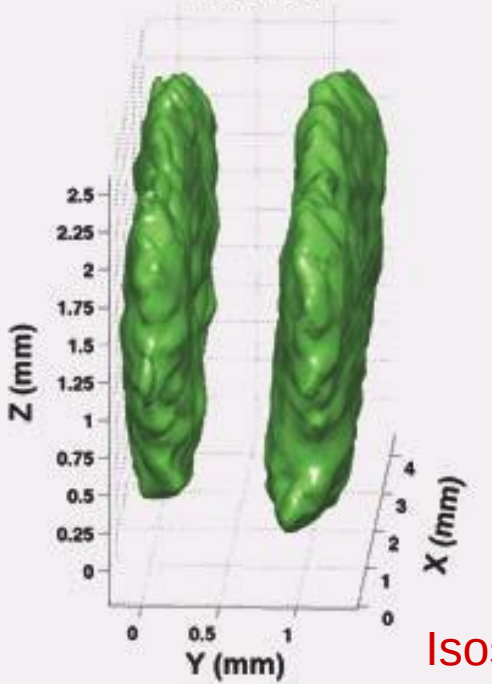

^{22}Na planar source edge-on
all angles, all gaps
1mm "mathematical" separation
MLEM reconstruction

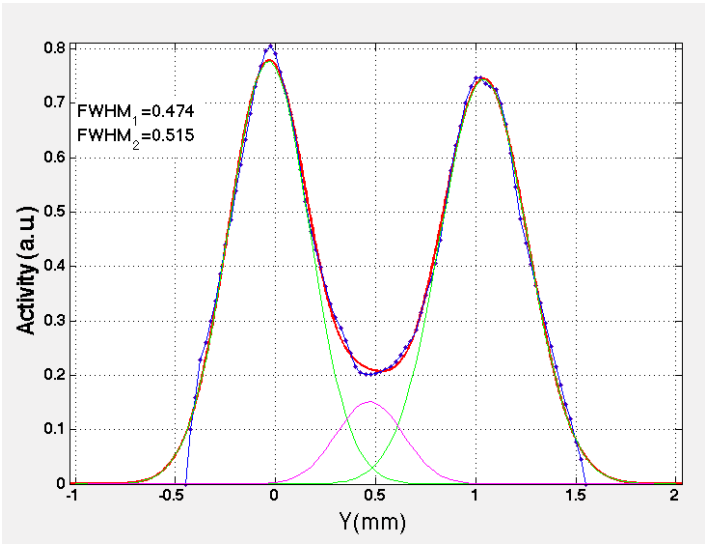

Profiles across image
(0.5 mm FWHM)

Isosufaces: 50% rel. activity

Resolution in final geometry (2 heads only, needle source)

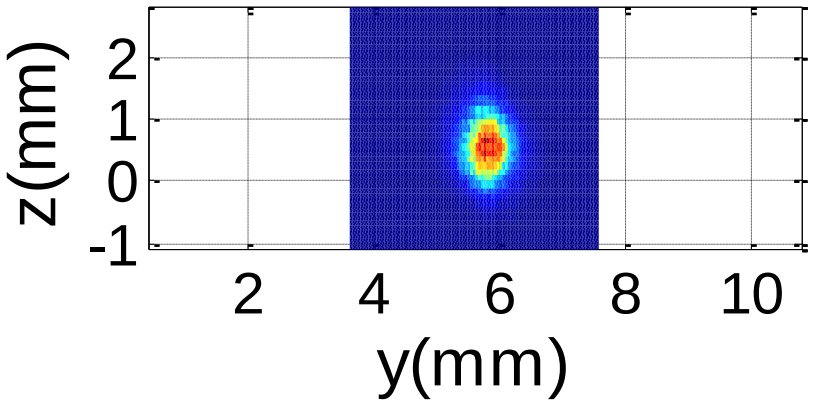

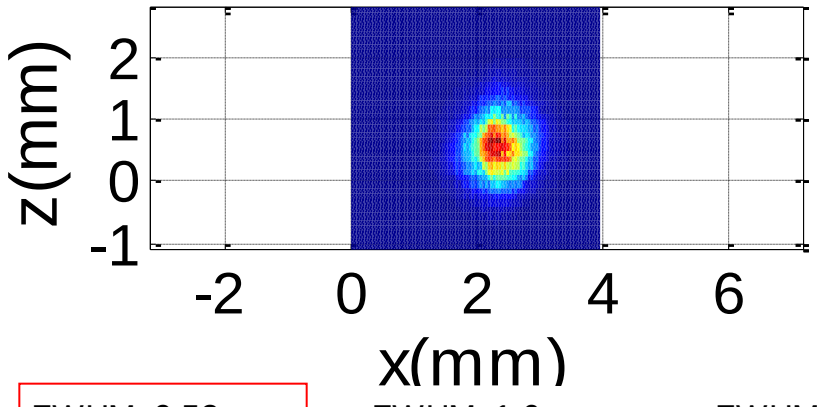

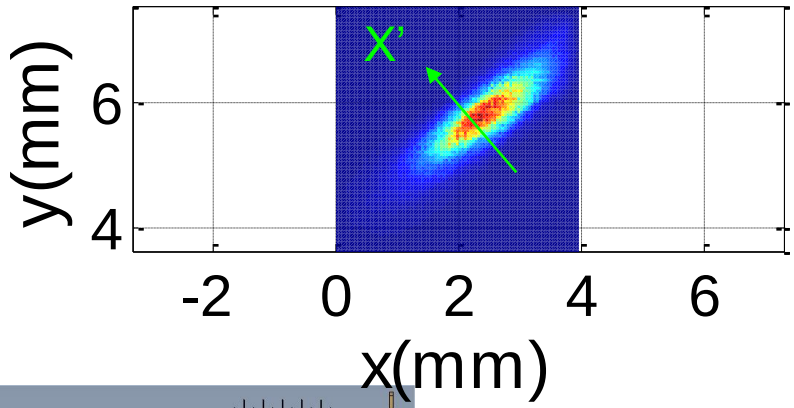

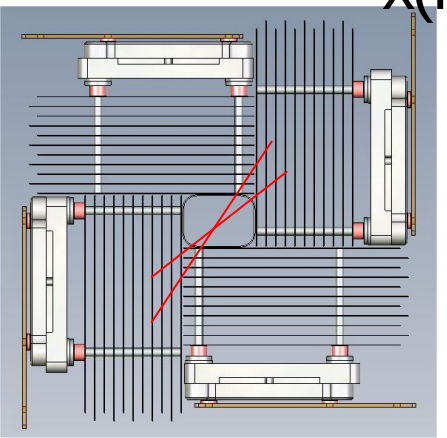

PRELIMINARY
Calibration not done in full.

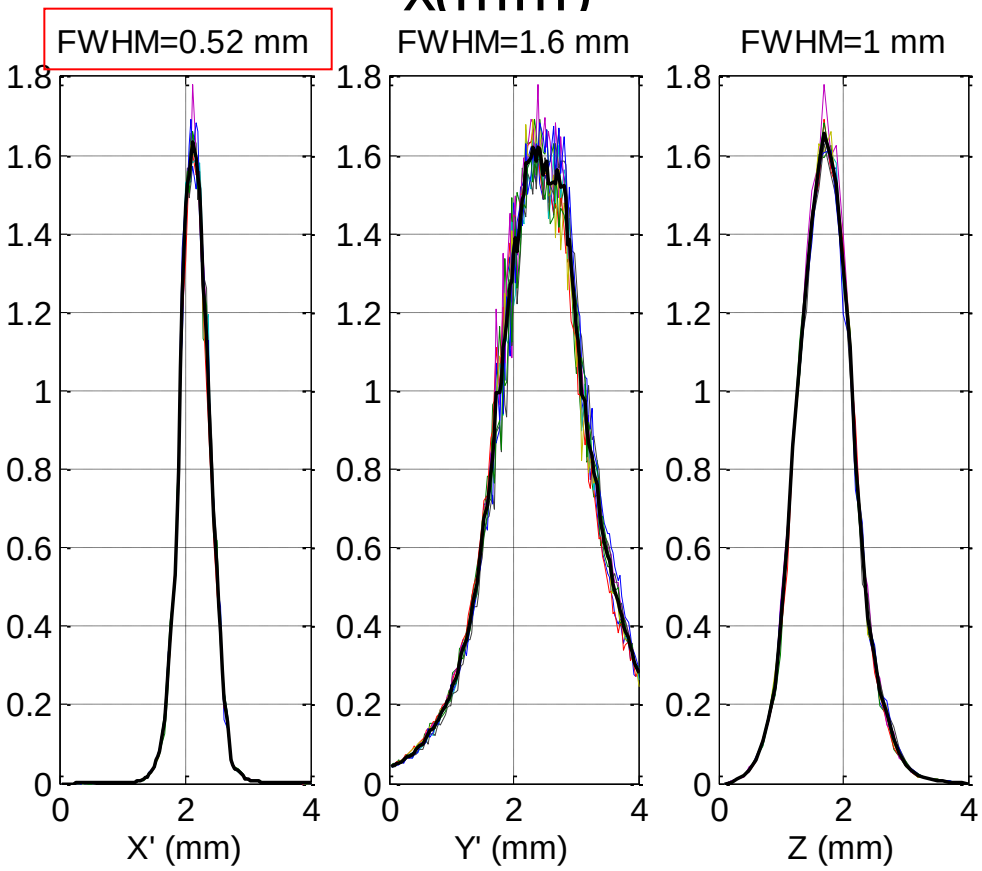

Full-body human RPC TOF-PET

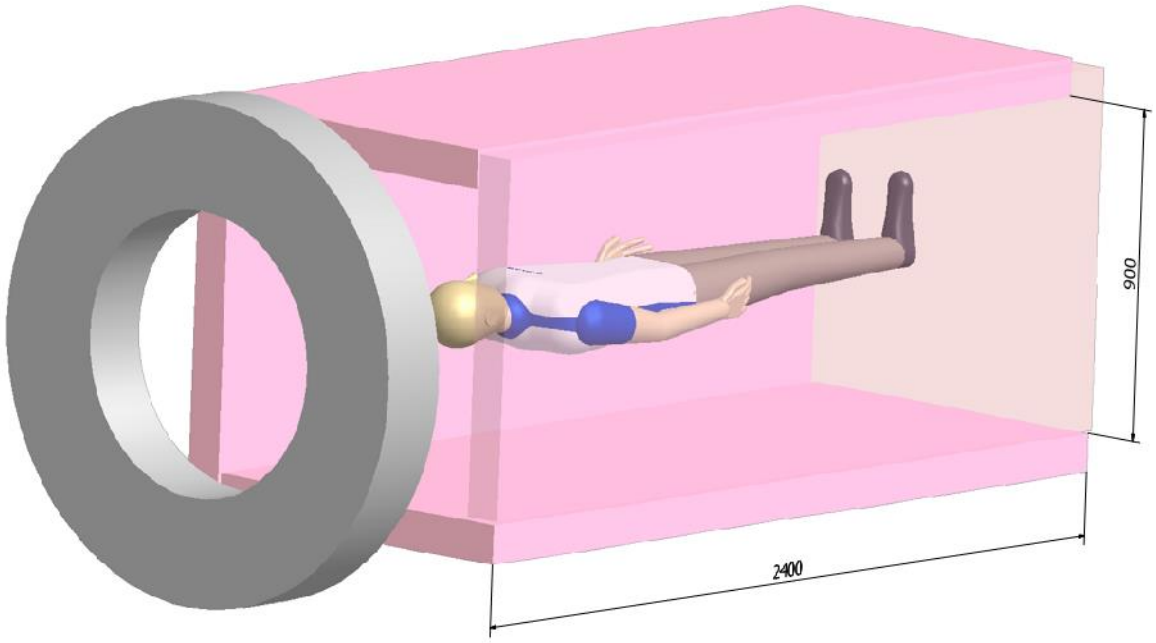

1) NECR – Noise Equivalent Count Rate

a) Simulation Setup

- Simulations performed with GEANT4, release 9.2, patch 4
- Scanner with parallelepipedic shape, with 4 detection walls, each of them containing 20 RPC detectors (~2400x1000x6.8 mm), with 10 gaps (350 μm thick) and glass resistive electrodes (200 μm thick)
- NEMA NU2–2001 Scatter Fraction Phantom centered in the Field Of View
- Source consists on the decay of ^{18}F at rest, uniformly distributed in the phantom line source, with photon non-collinearity provided by GATE

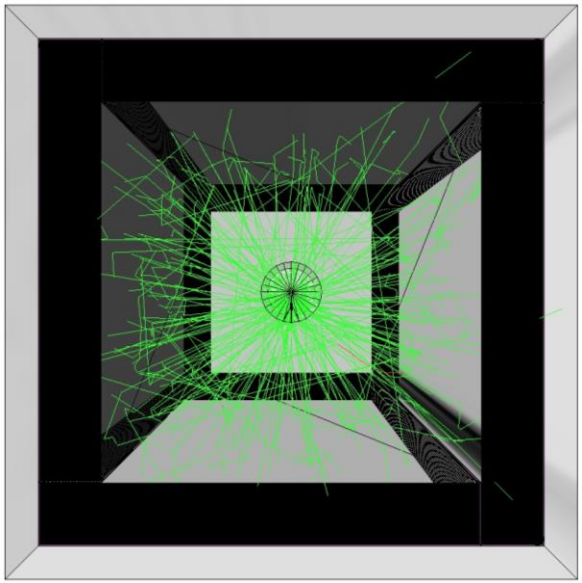

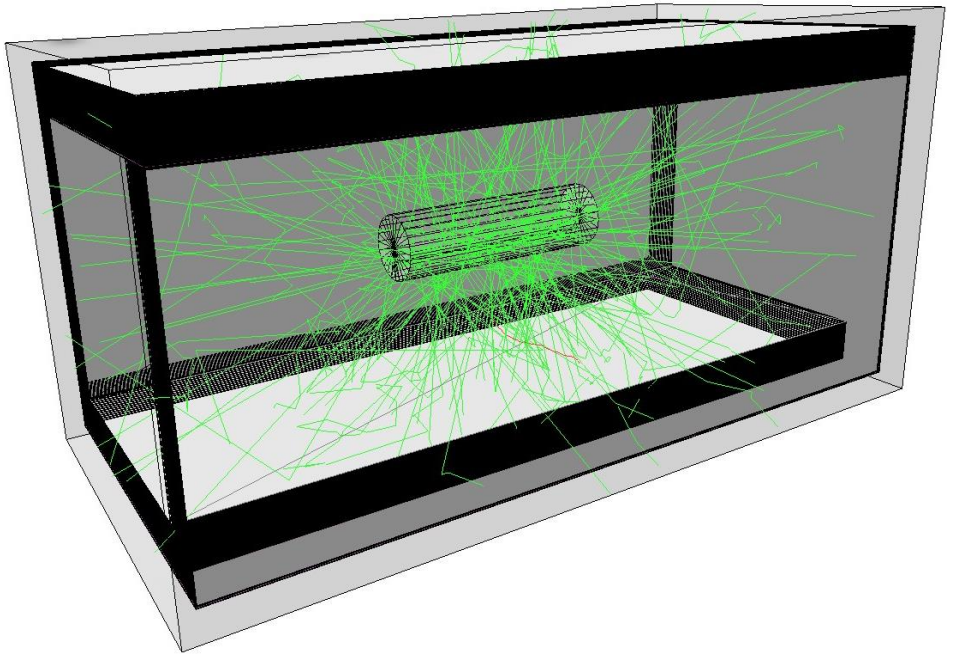

[M.Couceiro PhD thesys]

Calculations performed at the MILIPEIA cluster of Laboratório de Computação Avançada of U.C.

1) NECR – Noise Equivalent Count Rate

c) Phantom Geometry

- Solid right circular cylinder
  - Material: polyethylene with 0.96 specific gravity
  - Dimensions: 20 cm outside diameter and 70 cm overall length
  - Source: right circular cylinder with 3.2 mm inside diameter and 70 cm length, filled with ^{18}F diluted in water

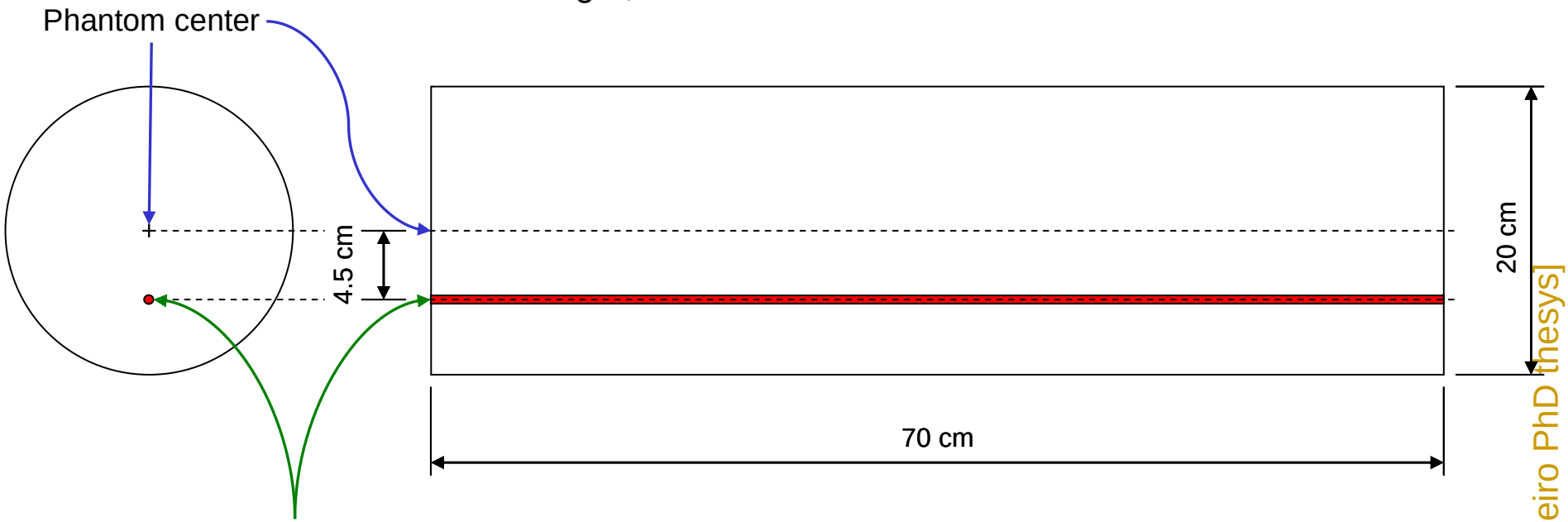

Line source with 3.2 mm inside diameter filled with ^{18}F diluted in water

(Dimensions in scale)

[M.Couceiro PhD thesys]

Readout strategy

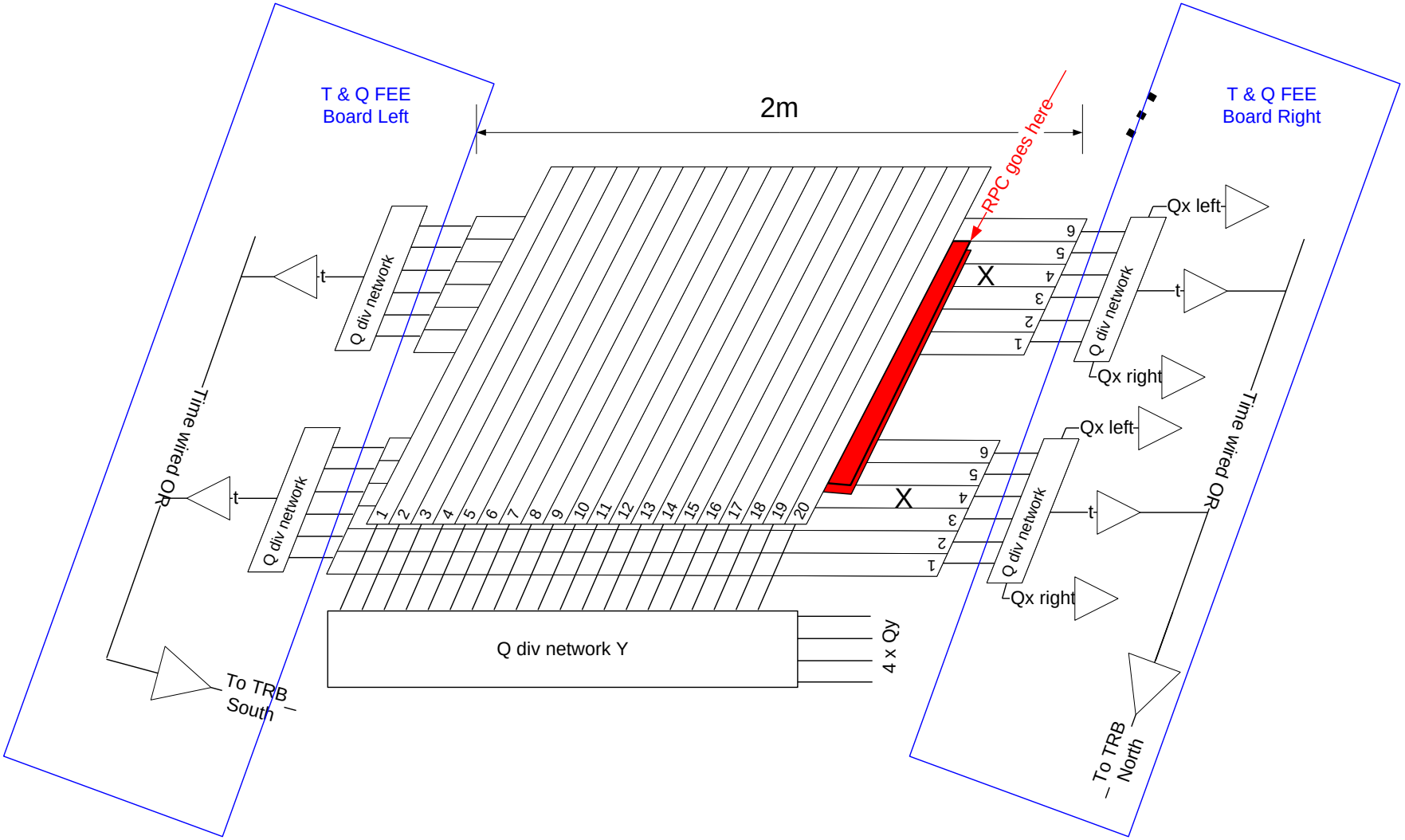

Scanner is composed by 800 independent readout “sections”, each measuring XY position and time for a single hit.

[Patent pending]

1) NECR – Noise Equivalent Count Rate

e) Multiple Hits Rejection

- After readout processing, multiple photon hits are removed by time-space considerations

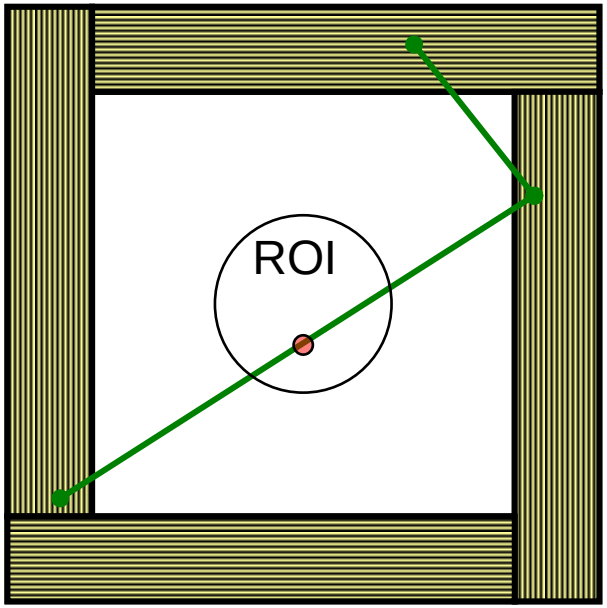

Scatter Fraction profiles for the axially extended phantom.

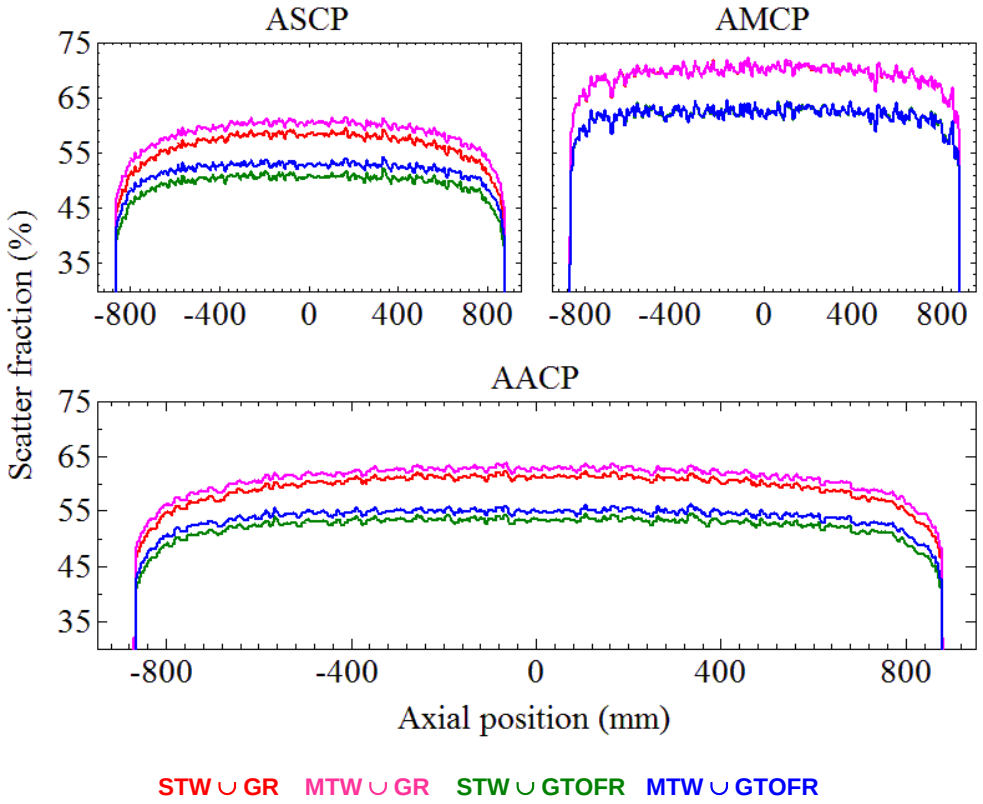

[M.Couceiro PhD thesys; P.Martins et al.,2012 IEEE NSS/MiC]

1) NECR – Noise Equivalent Count Rate

Clinical range

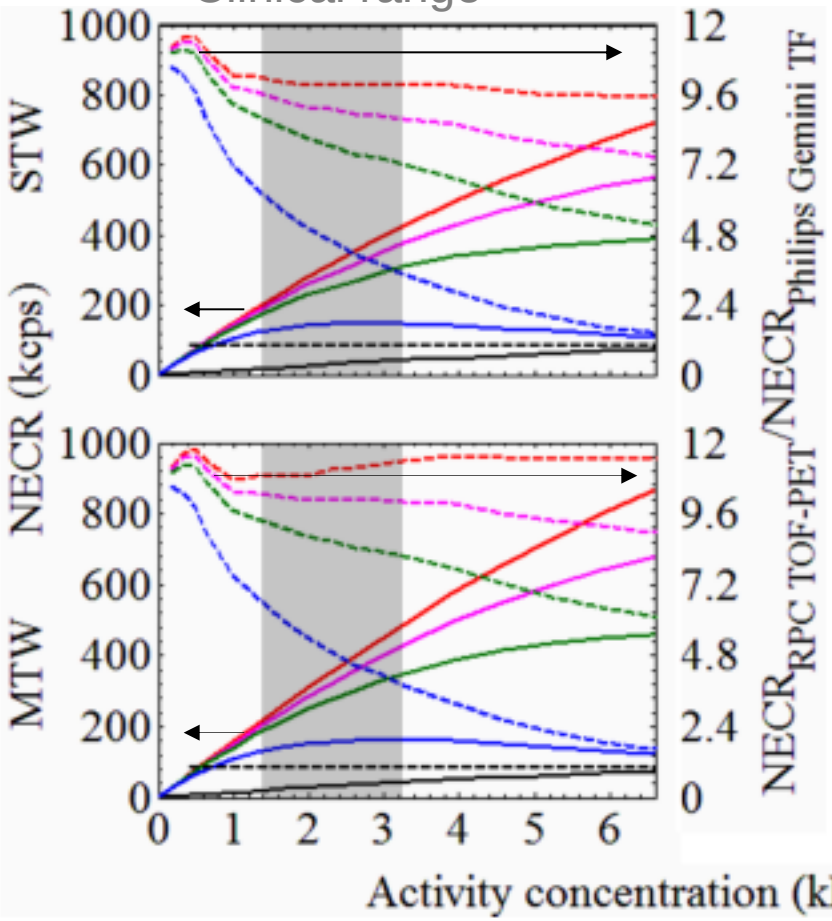

NEMA NU2-2001 - like
+ extra dead time for fine position

No TOF advantage considered
No single-bed advantage

Factors 5 to 11 NECR advantage over GEMINI TF
(depending on electronics dead time)

$$NEC = \frac{T^2}{T + S + 2R}$$

[M.Couceiro PhD thesys]

$\tau_{ps} = 0.0\ \mu s$ $\tau_{ps} = 0.5\ \mu s$ $\tau_{ps} = 1.0\ \mu s$ $\tau_{ps} = 3.0\ \mu s$

$NECR \rightarrow$ left Y axes

$\frac{NECR_{RPC\ TOF-PET}}{NECR_{Phylips\ Gemini\ TF}} \rightarrow$ right Y axes

Prototype detecting head (30×30cm^2 × 8 gaps)

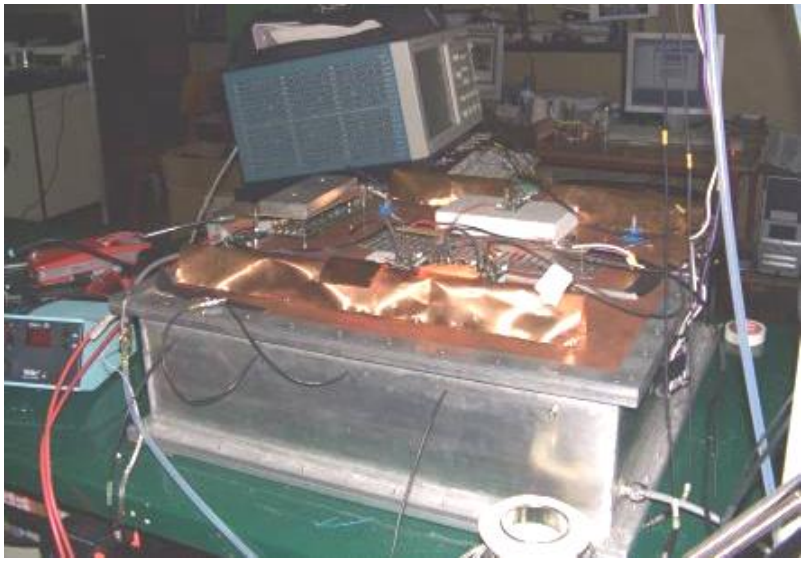

Time resolution – 300 ps FWHM

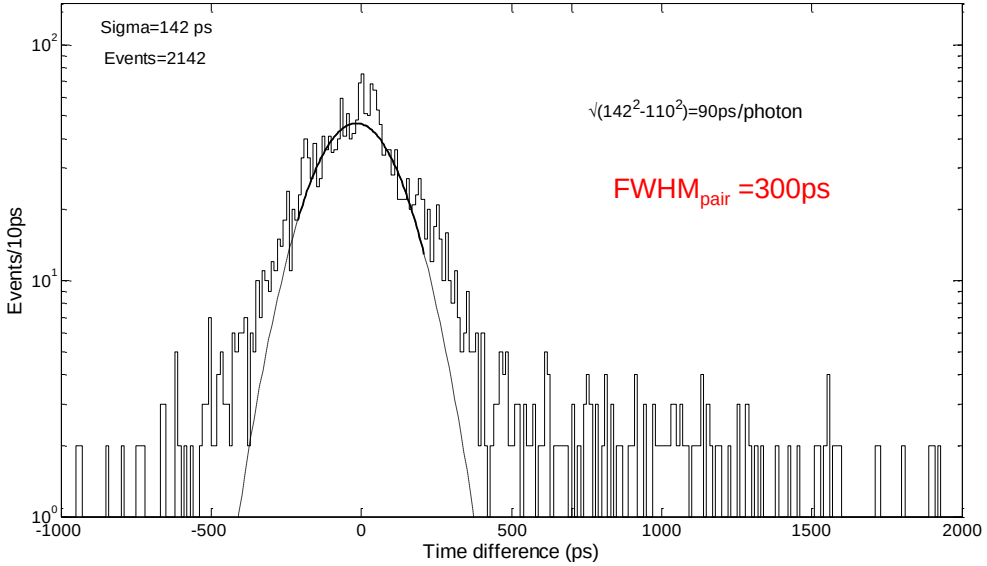

Efficiency as expected from GEANT

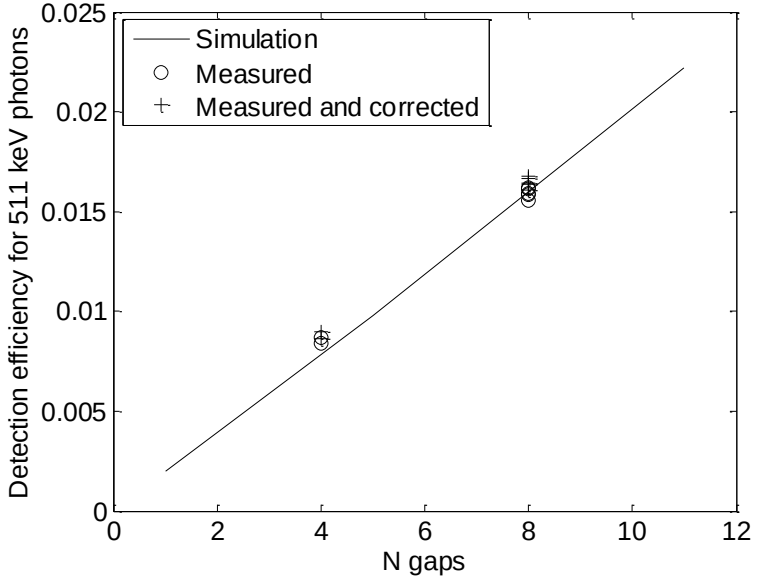

Reconstruction studies - Direct Time-of-Flight Whole Body 3D

NCAT Simulation (whole body)

Coronal

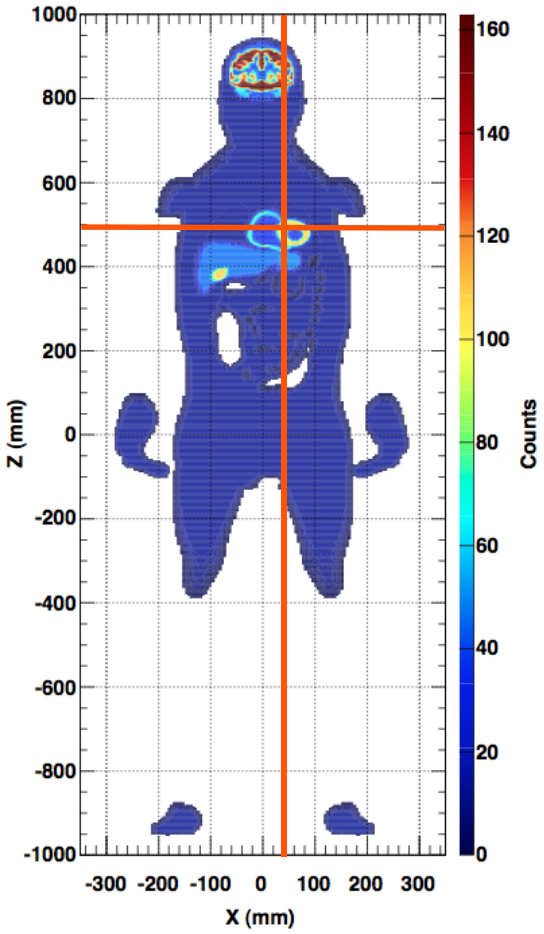

Sagittal

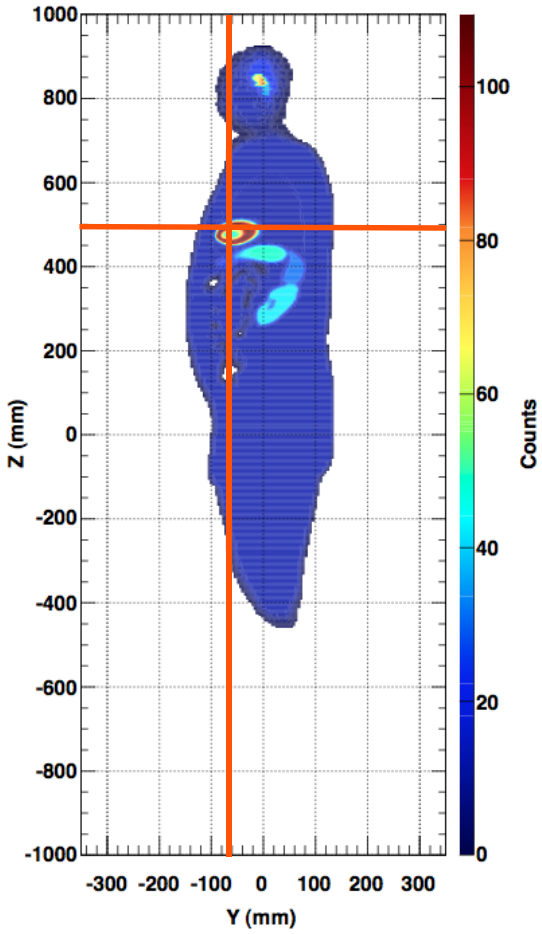

Axial

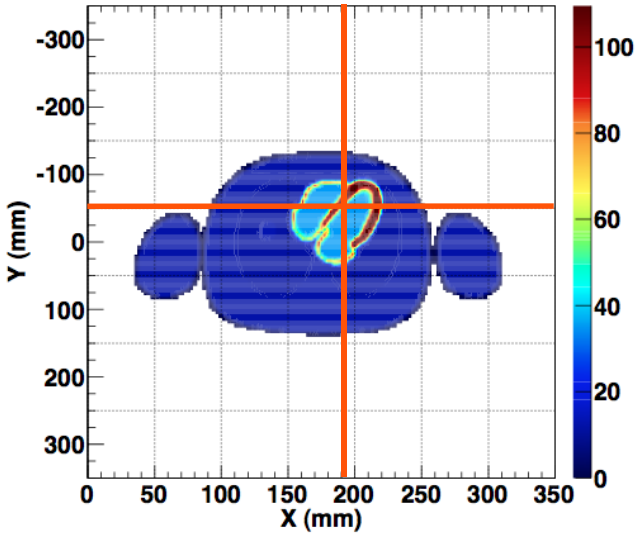

[P.Martins et al., IEEE MIC 2011]

Reconstruction studies - Direct Time-of-Flight Whole Body 3D

Backprojected Image (300 ps FHWM kernel)

Image quality suggests potential real-time imaging capability of RPC-PET

Coronal

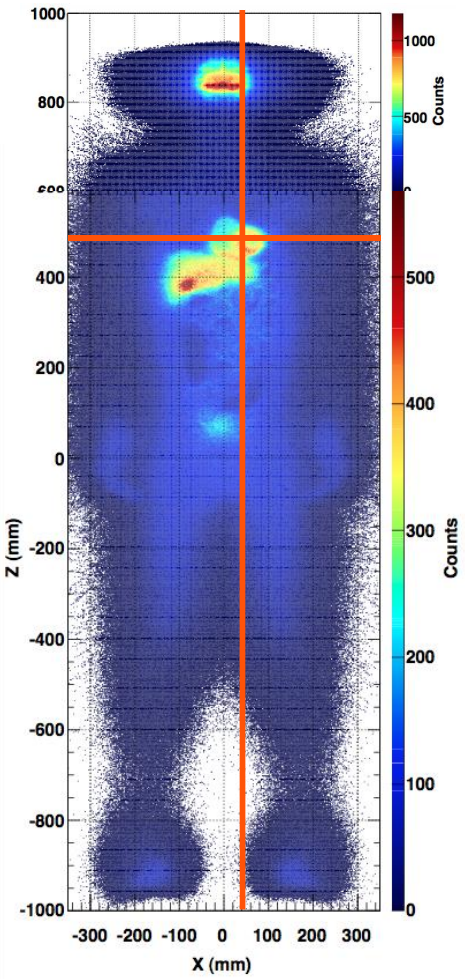

Sagittal

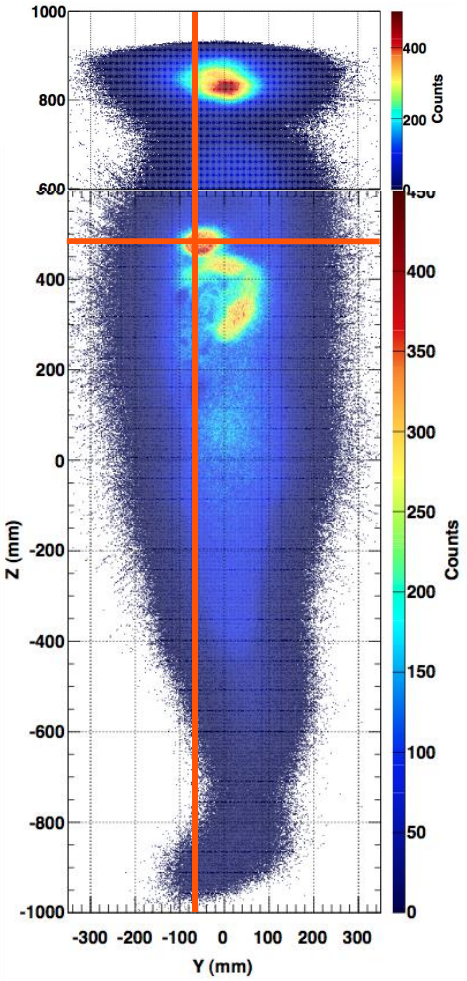

Axial

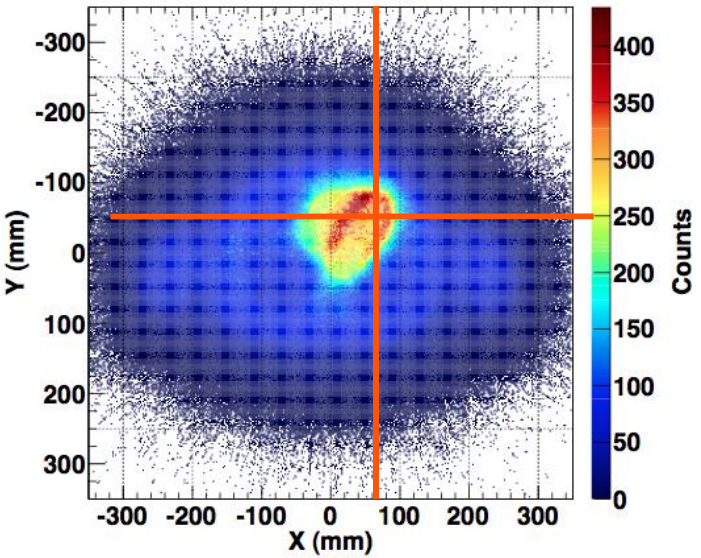

[P.Martins et al., IEEE MIC 2011]

Reconstruction studies - Direct Time-of-Flight Whole Body 3D

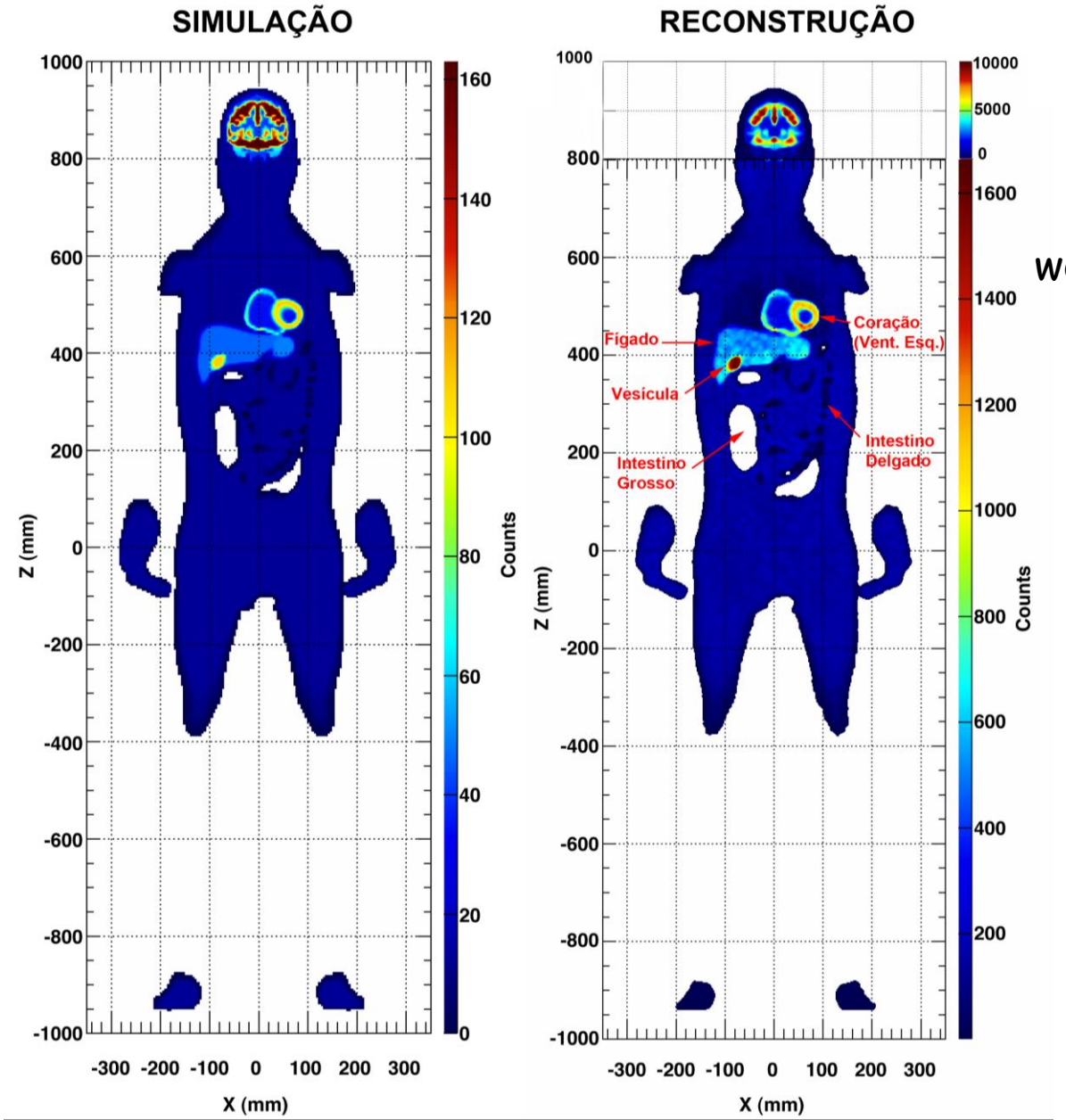

MLEM – 45 iterations

Full body 3D reconstruction in 7 minutes in a single workstation with 2 TESLA GPUs

[P.Martins et al., IEEE MIC 2011]

Reconstruction studies - Direct Time-of-Flight Whole Body 3D

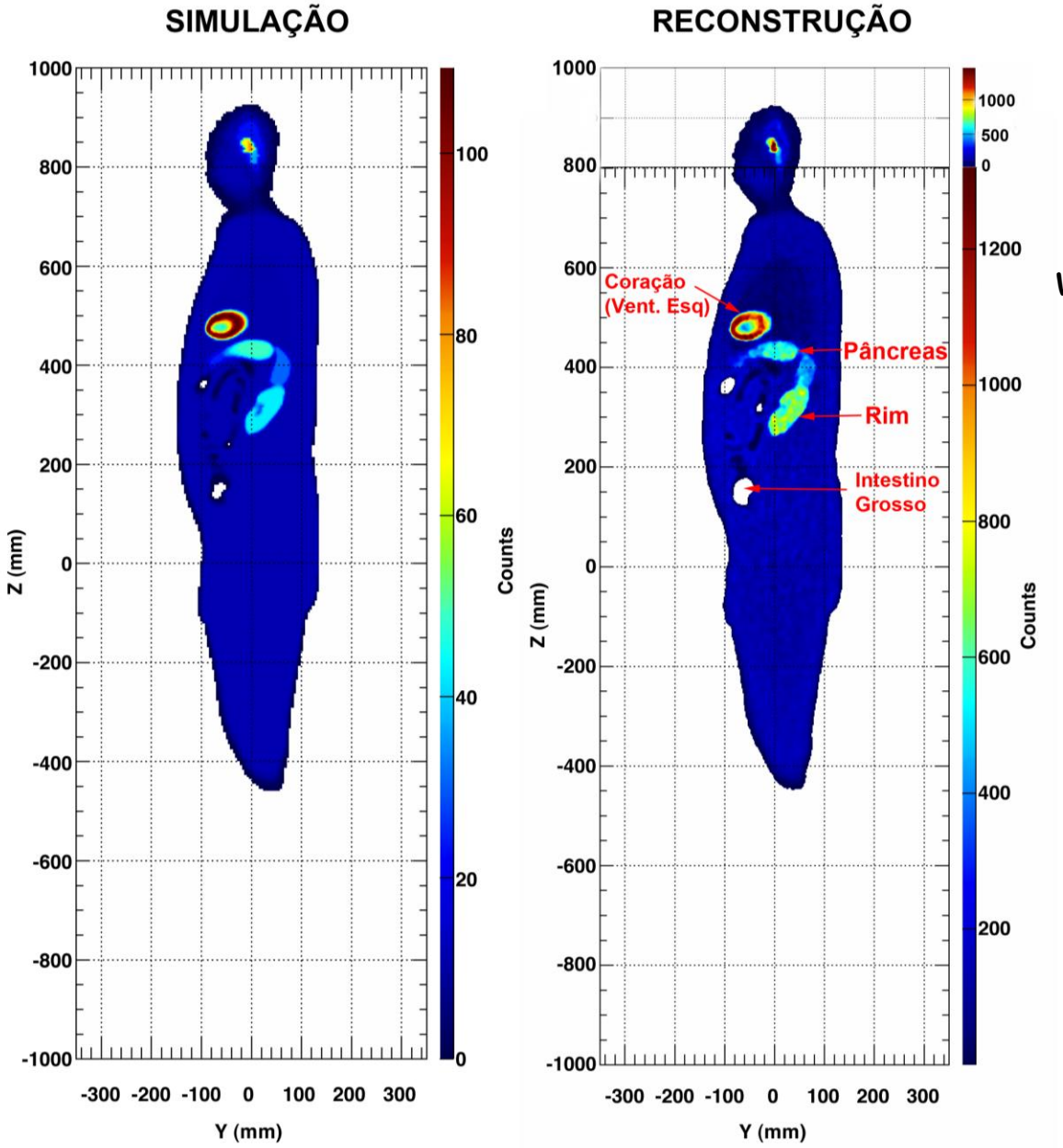

MLEM – 45 iterations

Full body 3D reconstruction in 7 minutes in a single workstation with 2 TESLA GPUs

[P.Martins et al., IEEE MIC 2011]

Reconstruction studies - Direct Time-of-Flight Whole Body 3D

MLEM – 45 iterations

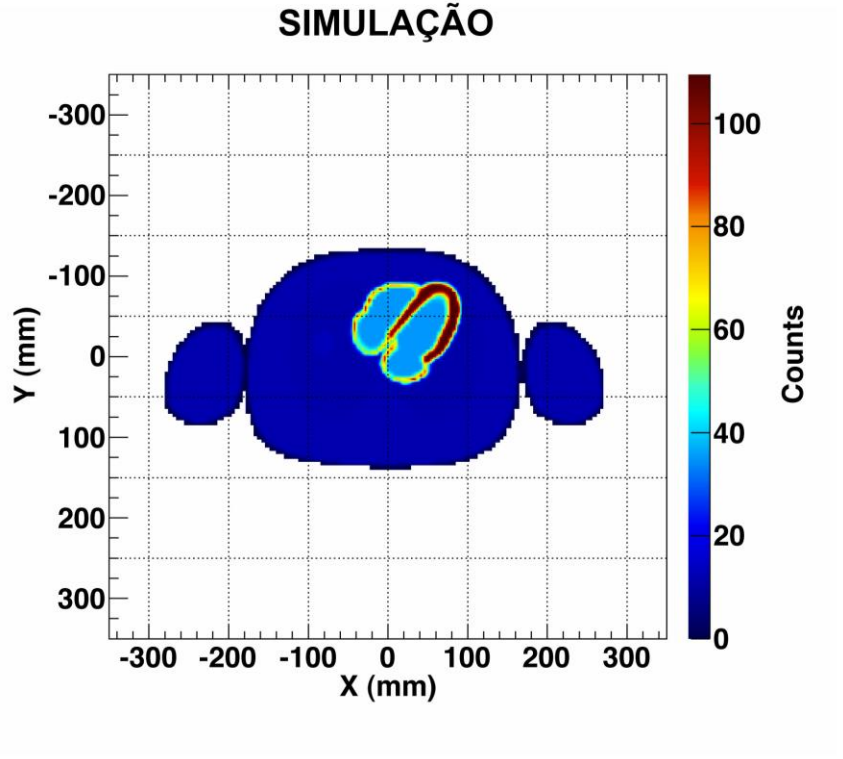

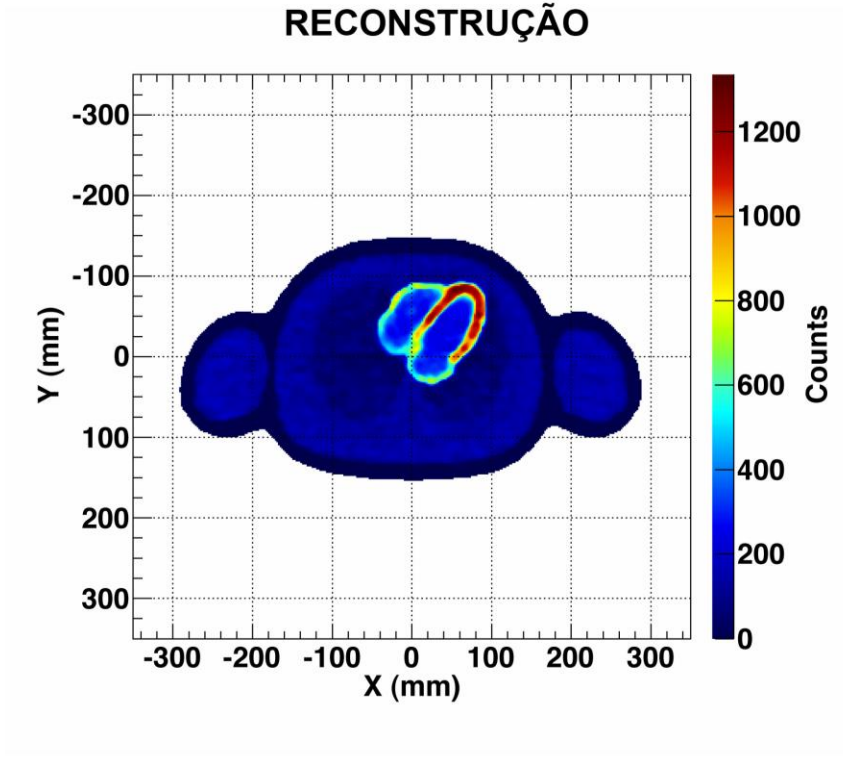

Full body 3D reconstruction
in 7 minutes in a single
workstation with 2 TESLA GPUs

[P.Martins et al., IEEE MIC 2011]

Reconstruction studies - Direct Time-of-Flight Whole Body 3D

300 ps TOF

600 ps TOF

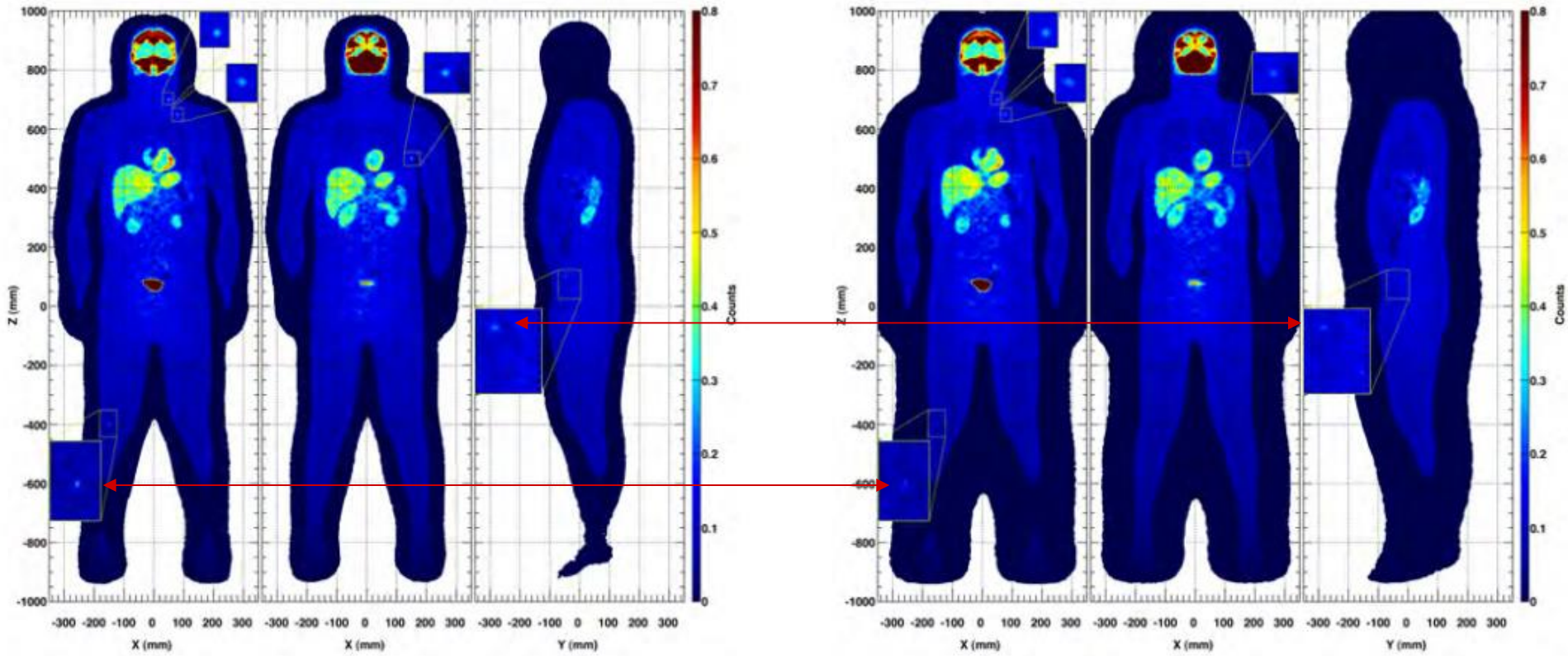

Fig. 15. Reconstructed images of the data detected by an RPC-PET system after including the scattered events and performing the rejection cuts with a 300 ps (left) and a 600 ps (right) FWHM TOF kernel. The abdominal region is more contaminated by scatters, however this region becomes cleaner due to the scatter rejection properties of RPC-PET. The organs are still well separated: the heart from the stomach, and the right kidney from the liver. The spleen is still visible. The constrast improves in all the lesions for a 300 ps FWHM TOF resolution (left), mainly the inguinal one, which is almost undistinguishable with a 600 ps FWHM TOFresolution (right).

Showing that TOF resolution affects lesion detectability
(a contentious point in the literature)

[P.Martins et al., IEEE MIC 2011]

Summary

- Excelling in large-area coverage with very good position resolution, gaseous detectors have very good perspectives for muon tomography applications
  - Geo-tomography (volcanoes, mining)
  - Security scans of containers against nuclear smuggling
- Applications in PET scanning (medicine) are being pursued with Resistive Plate Chambers:
  - Whole-body single-bed human TOF-PET
    - NEMA NU-2 2001 simulations suggesting **factors 5 to 11 NECR in advantage over GEMINI TF** (depending on assumed electronics dead time) without (hopefully) extra cost and excellent position resolution
    - Real-time biodynamics of the radiotracer (continuous uptake signal)
  - High resolution small-animal PET
    - **0.4 mm resolution demonstrated in realistic geometry, including DOI measurement;** 0.5 mm (preliminary) in the final scanner geometry
    - Simulations suggest that a **competitive peak NEC of 318 Kcps** may be obtained
  - Direct Time-of-Flight Whole Body 3D image reconstruction demonstrated in 7 minutes in a single workstation (important for both applications)